Washington University in St. Louis

Washington University Open Scholarship

McKelvey School of Engineering Theses & Dissertations

McKelvey School of Engineering

Fall 2022

Validation and Verification of the Wray-Agarwal Turbulence and Algebraic Transition Models for 2D External Airfoil Flows

Dean Ryan-Simmons

Follow this and additional works at: https://openscholarship.wustl.edu/eng_etds

Part of the Aerodynamics and Fluid Mechanics Commons

Recommended Citation

Ryan-Simmons, Dean, "Validation and Verification of the Wray-Agarwal Turbulence and Algebraic Transition Models for 2D External Airfoil Flows" (2022). *McKelvey School of Engineering Theses & Dissertations*. 770.
https://openscholarship.wustl.edu/eng_etds/770

This Thesis is brought to you for free and open access by the McKelvey School of Engineering at Washington University Open Scholarship. It has been accepted for inclusion in McKelvey School of Engineering Theses & Dissertations by an authorized administrator of Washington University Open Scholarship. For more information, please contact digital@wumail.wustl.edu.

WASHINGTON UNIVERSITY IN ST. LOUIS

McKelvey School of Engineering

Department of Mechanical Engineering & Materials Science

Thesis Examination Committee:

Ramesh K. Agarwal, Chair

Swami Karunamoorthy

David A. Peters

Validation and Verification of the Wray-Agarwal Turbulence and Algebraic Transition Models for 2D External Airfoil Flows

by

Dean M. Ryan-Simmons

A thesis presented to the McKelvey School of Engineering

of Washington University in

partial fulfillment of the requirements for the degree

of Master of Science

December 2022

St. Louis, Missouri

© 2022, Dean Ryan-Simmons

Table of Contents

List of Figures iv
List of Tables vi
Acknowledgments vii
Abstract ix
Chapter 1: Introduction 1
1.1 Background and Motivation 1
1.2 Scope of Thesis 3
Chapter 2: Introduction to Turbulence and Transition Modeling 6
2.1 Introduction to Turbulence Modeling 6
2.2 Introduction to Transition Modeling 8
2.3 Validation vs. Verification 9
2.4 References 10
Chapter 3: Validation of the Wray-Agarwal 2017 Turbulence Model for Symmetric NACA Airfoils 12
3.1 Introduction 12
3.2 Mesh Generation and Mesh Independence of Solution Study 12
3.3 Results 14
3.3.1 Comparison of Lift and Drag Coefficients 14
3.3.2 Comparison of Pressure Distributions 18
3.4 Conclusions 21
3.5 References 21
Chapter 4: Validation of the Wray-Agarwal Algebraic Transition Model for Symmetric NACA Airfoils 23
4.1 Introduction 23
4.2 Computational Methodology 24
4.2.1 Transition Models 25
4.2.2 Wray-Agarwal Algebraic Transition (WA-AT) Model 25
4.2.3 Mesh Generation 28
4.2.4 Mesh Independence of Solution Study 28

4.2.5 Convergence Criteria 30
4.3 Results 31
4.3.1 NACA 0012 Airfoil 32
4.3.2 NACA 0015 Airfoil 36
4.4 NACA 0018 Airfoil 39
4.5 Conclusions 40
4.6 References 42
Chapter 5: Application of the Wray-Agarwal Turbulence Model for Flow past Joukowski Airfoil: High Fidelity CFD Workshop 2022 Verification Case 44
5.1 Introduction 44
5.2 Computational Methodology 45
5.2.1 Mesh Generation 45
5.2.2 Flow Conditions 46
5.3 Results 46
5.3.1 First-Order Solution on Hexahedral Meshes 47
5.3.2 Second-Order Solution on Hexahedral Meshes 50
5.4 Conclusions 53
5.5 References 54
Chapter 6: Summary 55
Appendix A 57

List of Figures

Figure 1: Structured mesh around 2D NACA 0012 airfoil 13
Figure 2: NACA 0012 lift coefficient curves (left) and drag coefficient curves (right) using SA and WA models and their comparison with experimental data of Ladson [5], Re $6x10^6$. 15
Figure 3: NACA 0015 lift coefficient curve (left) and drag coefficient curve (right) using SA and WA models and their comparison with experimental data of Sheldahl and Klimas [6] at Re = $7x10^5$. 17
Figure 4: NACA 0018 lift coefficient curves (left) and drag coefficient curves (right) obtained with SA and WA models and their comparison to experimental data of Sheldahl and Klimas [6] at Re = $7x10^5$ 18
Figure 5: Computed pressure distributions on NACA 0012 airfoil using SA and WA model at α = 0 degree and their comparison with experimental data of with Gregory and O'Reilly [8]. 19
Figure 6: Computed pressure distributions on NACA 0012 airfoil using SA and WA model at α = 10 degree and their comparison with experimental data of with Gregory and O'Reilly [8]. 19
Figure 7: Computed pressure distributions on NACA 0012 airfoil using SA and WA model at α = 15 degree and their comparison with experimental data of with Gregory and O'Reilly [8]. 19
Figure 8: Numerical results for the NACA 0015 and 0018 airfoils at α = 0, 6, 12 degree angle of attack for Reynolds number = 7x10^5 20
Figure 9: Drag convergence study for the NACA 0012, 0015, and 0018 airfoils at Reynolds number = 5*10^5, turbulence intensity = 1% and viscosity ratio = 10. 29
Figure 10: (a) Computed skin-friction distribution (a) NACA 0018 airfoil, Reynolds number Re = 1*10^6, turbulence intensity Tu = 0.07%, α = 0°, experiment of Timmer 0, (b) NACA 0015, Reynolds number Re = 3*10^6, turbulence intensity Tu = 0.098%, α = 0°, experiment of Baek & Fugslang 0. 31
Figure 11: Computed transition location vs. angle of attack using the WA-AT and TSST models at Reynolds number Re = 3*10^6, turbulence intensity Tu = 0.3% and μt/μ = 100 compared to experiment of Gregory and O'Reilly [12]. 34
Figure 12: Computed lift coefficient vs. angle of attack using the TSST and WA-AT models at Reynolds number Re = 3*10^6, turbulence intensity Tu = 0.3% and μt/μ = 100 compared to experiment of Gregory and O'Reilly [12]. 34
Figure 13: Comparison of drag coefficient prediction using the TSST and WA-AT model with experiment of Gregory and O'Reilly [12], Re = 3*10^6. 35
Figure 14: Drag polar comparison using the WA-AT and TSST model with results of Barroullet et al. [14] and experiment of Gregory and O'Reilly [12], Re = 3*10^6. 35

Figure 15: Comparison of pressure coefficient distribution using the WA-AT and TSST model with the experimental data of Gregory and O'Reilly [12], Reynolds number Re = 3*10^6, turbulence intensity Tu = 0.3% and $\mu t/\mu$ = 100. 35
Figure 16: Comparison of transition location predictions using WA-AT and TSST model with the numerical results of Yousefi & Razeghi [13] and the experimental results of Baek and Fugslang [11], Re = 3*10^6, Tu= 0.098%. 37
Figure 17: Comparison of transition location predictions using WA-AT and TSST model with the numerical results of Yousefi & Razeghi [13] and the experimental results of Baek and Fugslang [11], Re = 6*10^6, Tu= 0.108%. 37
Figure 18: Skin friction distribution on the NACA 0015 airfoil at Re = 3*10^6 and (a) $\alpha = 0^o$ and (b) $\alpha = 6^o$; experimental transition location is from Baek & Fugslang [11]. 38
Figure 19: Transition location predictions using the TSST model for turbulent viscosity ratio ($\mu T/\mu$) = 1, 10, and 100; Re = 3*10^6 , Turbulence intensity Tu = 0.098%. 38
Figure 20: Comparison of transition location on NACA 0018 airfoil at Re = 1*10^6 and turbulence intensity Tu = 0.07% using TSST and WA-AT model with numerical results of Yousefi & Razeghi [13]and experimental data of Timmer [10]. 40
Figure 21: Comparison of lift coefficient of NACA 0018 airfoil at Re = 1*10^6 and turbulence intensity Tu = 0.07% using TSST and WA-AT model with experimental data of Timmer [10]. 40
Figure 22: Joukowski airfoil geometry and grid # 1 using boundary conditions from [1]. 46
Figure 23: Grid and error ('w.r.t truth value') convergence study of the total drag coefficient, first-order solution. 49
Figure 24: Convergence study of pressure and viscous drag coefficients, first-order solution. ... 50
Figure 25: Grid convergence study of the total drag coefficient, second-order solution. 52
Figure 26: Convergence study of pressure and viscous drag coefficients, second-order solution. 53

List of Tables

Table 1: Grid independence study of solution for NACA 0012 airfoil at Reynolds number = $6x10^6$ and angle of attack α = 8° using SA model. Error in lift coefficient is calculated against experimental data from Ladson [5]. 14
Table 2: Grid independence study of solution for NACA 0015 airfoil for Reynolds number = $7x10^5$ and angle of attack α = 8°. Error in lift coefficient is calculated against experimental data from Sheldahl & Klimas [6]. 14
Table 3: Grid independence study of solution for NACA 0018 airfoil for Reynolds number =$7x10^5$ and angle of attack α = 8°. Error in lift coefficient is calculated against experimental data from Sheldahl & Klimas [6]. 14
Table 4: Average errors in lift and drag coefficients for NACA 0012 airfoil at Re $6x10^6$, Ma = 0.15 for α ranging from -4.01 to 16.16 degrees when compared to experimental data of Ladson [5]. 15
Table 7: Mesh node distributions and mesh spacing *h* for six different meshes from coarse to fine. 30
Table 8: NACA 0012 airfoil: convergence study of drag coefficient C_D at Reynolds number = 5*10^5. 30
Table 9: NACA 0015 airfoil: convergence study of drag coefficient CD at Reynolds number = 5*10^5. 30
Table 10: NACA 0018 airfoil: convergence study of drag coefficient C_D at Reynolds number = 5*10^5. 30
Table 11: Effect of turbulent viscosity ratio μt/μ on flow characteristics for the Transition SST (TSST) model at Reynolds number Re = 3*10^6, turbulence intensity Tu = 0.3%, α = 0°. 33
Table 12: Convergence of total, pressure and viscous drag coefficients for first-order solution on grid #0 to grid #6. 48
Table 13: Convergence of total, pressure and viscous drag coefficients for second-order solution on grid #0 to grid #6. 51

Acknowledgments

First and foremost, I would like to acknowledge my advisor, Professor Ramesh K. Agarwal, for his unwavering encouragement and leadership during investigation of this research study. Dr. Agarwal's devotion and pursuit of new challenges has illuminated a rewarding career path for me. Through his guidance, I have learned about aerodynamics research, methods for solving fluid dynamics problems, and have developed a passion for pursuing new set of challenges.

I would like to acknowledge the committee member, Dr. Peters and Dr. Karunarmoorthy, for taking the time to read this thesis and attend the defense. I would also like to thank the National Science Foundation for the financial support, Grant Number (DGE-2139839).

Dean M. Ryan-Simmons

Washington University in St. Louis

December 2022

Dedicated to my mother and grandparents.

ABSTRACT OF THE THESIS

Validation and Verification of the Wray Agarwal Turbulence and Transition Model

For 2D External Airfoil Flow

by

Dean M. Ryan-Simmons

Master of Science in Aerospace Engineering

Washington University in St. Louis, 2022

Professor Ramesh K. Agarwal, Chair

Validation and verification benchmark test cases are employed in computational fluid dynamics (CFD) to determine the best practices in application of various CFD tools. These cases focus on the geometry modeling, mesh generation, numerical algorithms, and turbulence models to ensure consistent and accurate numerical simulation of physical phenomena. Assessing model accuracy is essential to identify areas of improvement in various turbulence models. Flow past several symmetric NACA airfoils, namely NACA 0012, NACA 0015 and NACA 0018 are standard test cases for validating and evaluating turbulence models' accuracy since the experimental data is available for these airfoils. Available wind tunnel data allows for testing turbulence models' capability to predict lift, drag, and pressure distributions for various angles of attack ranging at high Reynolds numbers. In this study, two turbulence models are compared to experimental data for the NACA 0012, 0015, and 0018 airfoils. The two turbulence models are the well-known one equation Spalart-Allmaras (SA) and the recently developed Wray-Agarwal (WA) model. Numerical results show that both turbulence models are capable of accurately predicting lift and pressure coefficients but generally over predict drag. However, the WA model

exhibits higher accuracy in predicting lift at high angles of attack for two of the airfoils and peak pressure for NACA 0012 airfoil.

The Wray-Agarwal Algebraic Transition (WA-AT) model is a recently proposed new transition model with the goal to obtain similar level or better accuracy with substantially less computational cost compared to existing three (*k-kl-ω)* or four ($k - \omega - \gamma - Re_{\theta t}$) equation transition models. The WA-AT model uses the wall distance free version of WA turbulence model (WA2018) in combination with an algebraic transition model. The model has been previously validated for various ERCOFTAC benchmark flat plate cases and for some aerodynamic bodies. To further validate this model, the transitional flows past NACA 0012, 0015, and 0018 airfoils are simulated for a range of Reynolds numbers, turbulence intensities, and angles of attack in ANSYS Fluent. The NACA airfoil cases are simulated at angles of attack from zero to ten degrees, and Reynolds numbers ranging from $1 * 10^6$ to $6 * 10^6$, and turbulence intensities ranging from 0.07% to 0.3%. The validation studies show similar or improved predictions using the WA-AT model over the Langtry-Menter's four equation transition-SST ($k - \omega - \gamma$ - $Re_{\theta t}$) model for pressure, drag, lift, and transition location. Overall, the results demonstrate that the WA-AT model offers similar or better accuracy as the four-equation transition-SST model for simulation of transitional flow over NACA 0012, 0015, and 0018 airfoils at much less computational cost.

In NASA's High Fidelity CFD Workshop 2022, the Joukowski airfoil was identified as a benchmark verification case to test the convergence behavior of different turbulence models in different CFD solvers with particular emphasis on SA-neg-QCR 2000 turbulence model. This thesis also studies the accuracy and convergence behavior of Wray-Agarwal (WA) and Spalart-Allmaras (SA) one equation turbulence models by computing the flow past Joukowski airfoil on

a sequence of seven workshop specified grids from coarse to fine. The benchmark case has free stream Mach number of 0.15, chord Reynolds number of $3x10^6$ and angle of attack of 0 degree. The goal is to evaluate the convergence behavior of drag coefficient on a sequence of seven grids using WA and original version of SA model in ANSYS Fluent. Both models exhibit nearly first order convergence rates for first order solutions and second order convergence rates for second order solutions. There is no notable difference in the convergence rates between the two turbulence models for both first order and second order implementations.

Chapter 1: Introduction

This chapter provides background of the Computational Fluid Dynamics application to two-dimensional external flows past airfoils. The motivation behind verification and validation of turbulence and transition models is discussed. This research demonstrates the accuracy and capability of single transport equation turbulence and transition models. The scope of the thesis is also described in this section.

1.1 Background and Motivation

Computational fluid dynamics (CFD) is the most efficient and affordable tool for design and development of technologies that involve fluid flows. The Navier-Stokes equations, along with continuity and energy equation can model the viscous flow and heat transfer in a fluid domain. The high non-linearity of Navier-Stokes equations makes it very difficult if not impossible to have analytical or semi-analytical solutions of the equations for complex geometries. CFD utilizes several building block tools, namely, geometry modeling, grid generation, numerical algorithms for the solution of the governing equations of fluid dynamics. Numerical algorithms often include turbulence modeling as an additional building block objective. An appropriate physical model and associated governing equations must be chosen to describe the physics of a problem. As with any mathematical model, one must make sure that the physics of the problem is modeled correctly and the model is solved correctly using the appropriate boundary conditions. There are different levels of numerical complexity that occur in computational fluid dynamics depending upon the complexity of flow physics. For example, if the viscous effects are not important in a flow, Navier-Stokes equations can be simplified to Euler equations and if the

fluid density is constant and the flow field is irrotational, the governing equations simply become the Laplace equation for velocity potential.

However, for turbulent flows, there are currently three approaches/models – the Reynolds-Averaged Navier Stokes (RANS) equations, the Large-Eddy Simulation (LES) and Direct Numerical Simulation (DNS). For 3D industrial applications, RANS equations with a turbulence model is the most widely used approach since it is computationally less intensive compared to LES and DES and compute complex 3D turbulent flows at realistic Reynolds numbers on the currently available computing hardware. As is well known, the main drawback of RANS equations is that they are the result of Reynolds-Averaging of turbulent fluctuations which leads to the so called unknown turbulent or "Reynolds Stresses." This results is called the "Closure Problem." It implies that the Reynolds Stresses need to be modeled. The modeling of Reynolds Stresses is called "Turbulence Modeling."

Most turbulence models are empirical and use the concept of "eddy viscosity" defined by the Boussinesq assumption. For more than a century, many turbulence models have been developed which are called in the literature as zero-equation, one-equation, two-equation, four-equation, and full-Reynolds Stress models depending upon the number of turbulence variables used in describing the eddy viscosity. In this thesis, two one-equation turbulence models, namely the industry standard Spalart-Allmaras (SA) and recently developed Wray-Agarwal (WA) models are used for solution of RANS equations.

Direct Numerical Simulation (DNS) fully resolves the entire range of turbulent length scales. DNS requires excessive computational power that is not currently available to compute 3D flow at realistic Reynolds numbers. Large Eddy Simulation (LES) is a middle ground between RANS

and DNS, modeling small eddies in the flows using models such as “Smagorinsky” model and fully resolving other features of the turbulent flow.

As mentioned before, in this thesis, RANS equations are solved in conjunction with SA and WA model. It should be mentioned that to capture higher accuracy with lower computational cost, the Wray-Agarwal (WA) turbulence model was developed. This model attempts to capture the best aspects of two other two-equation turbulence models in one transport equation. It behaves like k-ε model in the far field and like k-ω model near the wall.

The transition from laminar to turbulent flow over an aerodynamic body significantly impacts lift, drag, pressure, velocity and other flow properties. In an age where range, efficiency, and emissions reductions of an airplane have become primary concerns in aviation, accurate modeling of turbulent and transitional flow allows for better optimization and design of future aircraft. The Wray-Agarwal Algebraic Transition (WA-AT) model offers a potential improvement over the current three or four equation transition SST models. The WA-AT model may offer the accuracy of a four transport equation transition model at the cost of one transport equation.

1.2 Scope of Thesis

The goal of this work is to validate and verify the accuracy and computational efficiency of Wray-Agarwal turbulence model through comparisons with available experimental and numerical data which may be based on other turbulence models such as Spalart-Allmaras (SA) and k-ω SST. The additional goal is to validate the recently developed Wray-Agarwal Algebraic Transition model. A summary of the contents of various chapters is given below:

Chapter 2: Introduction to Turbulence and Transition Modeling: This chapter introduces the common practices for validation and verification of turbulence models in computational fluid dynamics (CFD). Validation and verification is an essential part of the model development process to ensure that models are physically accurate and mathematically valid. The difference between validation and verification is explained, and the method to "validate" or "verify" the models is described. A brief description of the turbulence and transition models used in this thesis is also presented in this section.

Chapter 3: Validation of the Wray-Agarwal 2017 Turbulence Model for Symmetric NACA Airfoils: Validation cases for the NACA 0012, 0015, and 0018 airfoils are computed using the Wray-Agarwal turbulence model and are compared with experimental data and an industry standard SA turbulence model. The chapter describes the two turbulence models used, meshes generated and solutions using the Reynolds-Averaged Navier Stokes (RANS) equations and their comparison with experimental data.

Chapter 4: Validation of the Wray-Agarwal Algebraic Transition Model for Symmetric NACA Airfoils: Validation cases for the NACA 0012, 0015, and 0018 are computed using the Wray-Agarwal Algebraic Transition (WA-AT) model. Results from WA-AT and four-equation Transition SST (TSST) model are compared with experimental data for transition location, lift, drag, and pressure distribution at various Reynolds numbers and angles of attack.

Chapter 5: Application of Wray-Agarwal Turbulence Model for Flow Past Joukowski Airfoil: High Fidelity CFD Workshop 2022 Verification Case: Joukowski airfoil CFD verification case from High Fidelity CFD Workshop 2022 is used to test the convergence properties of Wray-Agarwal turbulence model on seven workshop prescribed meshes from coarse to fine using first-order and second-order algorithms in ANSYS Fluent and are compared

with those obtained using the SA model. This comparison provides insight into whether the Wray-Agarwal turbulence model is solved correctly in ANSYS Fluent. The solution convergence is evaluated on hexahedral meshes by comparing the convergence of total drag, viscous drag, pressure drag, and error in total drag on various meshes and the convergence properties results obtained from SA and WA model are compared.

Chapter 6: Summary: This chapter provides a summary of key results in the thesis and based on that describes the overall potential of the Wray-Agarwal turbulence and transition models.

Chapter 2:Introduction to Turbulence and Transition Modeling

2.1 Introduction to Turbulence Modeling

Turbulence is a fluctuating disorderly motion within a flow [1] and is present in all flows as an unsteady effect. As mentioned in Chapter 1, there are several mathematical/numerical approaches for characterizing turbulent flows with varying degree of fidelity, namely the Reynolds-Averaged Navier Stokes (RANS) equations, Large Eddy Simulation (LES) and Direct Numerical Solution (DNS). RANS solvers in conjunction with a turbulence model are widely used in the industry for design and optimization of products that involve turbulent fluid flow. Once validated, they can be very cost effective since they can reduce the amount of expensive wind-tunnel testing since a large number of configurations and flow conditions can be simulated in a short time with relatively less computational cost. However, RANS solvers require turbulence models which are empirical in nature and introduce inaccuracies and uncertainty in the computed results.

Most turbulence models are based on the concept of "eddy viscosity" defined by the Boussinesq assumption. For more than a century, many turbulence models have been developed which are called in the literature as zero-equation, one-equation, two-equation, four-equation, and full-Reynolds Stress models depending upon the number of turbulence variables used in describing the eddy viscosity. In this thesis, two one-equation turbulence models, the industry standard Spalart-Allmaras (SA), and recently developed Wray-Agarwal (WA) models are used for solution of RANS equations. These models solve a transport equation for linear eddy viscosity. The two equation models (k-ε, k-ω, SST k-ω, k-kL and others) use a transport equation

for turbulent kinetic energy and another equation for either turbulent dissipation or specific turbulent dissipation rate or turbulence length scale. The information about these models can be obtained from Ref. [1].

Here we now briefly describe the one-equation SA and WA model which are used in this thesis. The SA model is a transport equation that describes the turbulent viscosity in the flow. The equation was developed using empiricism, arguments of dimensional analysis, and few other considerations [2]. The coefficients in the model were fine-tuned using the experimental data. The transport equation for eddy viscosity can be written as [2]:

$$\frac{\partial}{\partial t}(\rho v) + \frac{\partial}{\partial x_i}(\rho v u_i) = G_v + \frac{1}{\sigma_v}\left[\frac{\partial}{\partial x_j}\left\{(\mu + \rho v)\frac{\partial v}{\partial x_j}\right\} + C_{b2}\rho\left(\frac{\partial v}{\partial x_j}\right)^2\right] - Y_v + S_v \qquad (1)$$

The details of the model are given in Ref. [2]. The SA model is very stable and is easy to implement in different CFD codes. The model is now a part of several commercial CFD codes, namely ANSYS, CFX, COMSOL among others and many industry and government labs developed CFD codes. The access of this model has led to implementations worldwide by researchers and practitioners. The description of the turbulent kinematic viscosity in Eq. (1) has shown great accuracy in computation of wall bounded flows with large pressure gradients but has also shown inaccuracies when the length scale changes due to transition between shear flow and wall bounded flow.

The Wray-Agarwal (WA) model is also a linear turbulent eddy viscosity model; it has a single transport equation derived from the k-ω SST closure [3]. The k-ω model is a two-equation turbulence model known for its accuracy in prediction of wall bounded flows with small regions of separation and in adverse pressure gradient boundary layers, which are common in the near wall regions of wall bounded external flows. The WA model utilizes a blending function that

allows the model to act as the one equation version of the k-ω model near the wall or the two-equation k-ε model in free stream region away from the wall.. The k-ε model is known for resolution of free shear flows and flows with small pressure gradients, but is known to struggle in the near wall region where the k-ω model excels. The WA model captures the benefits of both two equation models in a single equation. In CFD, the more equations you use to model a problem, theoretically, the more accurate the result should be. The advantage of WA model is higher accuracy with less computational expense than the standard two equation models. The $R = k/\omega$ (eddy viscosity) transport equation for the WA-2017 can be written as:

$$\frac{\partial R}{\partial t} + \frac{\partial u_j R}{\partial x_j} = \frac{\partial}{\partial x_j}\left[(\sigma_R R + v)\frac{\partial R}{\partial x_j}\right] + C_1 RS + f_1 C_{2k\omega}\frac{R}{S}\frac{\partial R}{\partial x_j}\frac{\partial S}{\partial x_j} - (1 - f_1)C_{2k\epsilon}R^2\left(\frac{\frac{\partial S}{\partial x_j}\frac{\partial S}{\partial x_j}}{S^2}\right) \quad (2)$$

Further details on the Wray-Agarwal turbulence model may be found in [3].

2.2 Introduction to Transition Modeling

The Wray-Agarwal Algebraic Transition (WA-AT) model introduces an algebraic intermittency gamma equation based on the formulation of Cakmakcioglu et al. [4]. The intermittency equation is used to describe the transition from laminar to turbulent flow. A common practice in transition prediction is to solve a second transport equation for the intermittency. An algebraic form of an equation for intermittency has been shown to significantly reduce the computational cost while maintaining good accuracy. Xue integrated the algebraic equation similar to that of Cakmakcioglu et al. into the WA2018 one-equation turbulence model [5]. The WA2018 model is the wall distance free version of the WA2017 model. A “wall distance free” version means that the model can be applied down to the wall (boundary condition) without explicit knowledge of the local distance from the wall [6]. This means that the

model can be applied to more complex geometries easily. There are few standard transition models frequently used, most of these models require three or more equations to accurately predict transition. The WA-AT model offers this transition prediction accuracy with just one equation. Full derivation of the WA-AT model is given in [5]. The WA-AT model is also described in detail in Chapter 4.

2.3 Validation vs. Verification

After the turbulence model is developed and calibrated, there are two key steps remain; validation and verification. Validation of a model is focused on how accurately the model can predict the physically realizable characteristics [7]. This means comparing numerical prediction to experimental data and to other well documented and reliable numerical predictions. There are several well-known validation benchmark cases often used in turbulence modeling literature. The flow past a flat plate is the simplest case to solve numerically and there is an abundance of experimental data available. For example, experimental and numerical results can be compared to the "seventh power law" solution of Prandtl for zero pressure gradient flow. Other benchmark 2D and 3D validation cases can be found on the NASA Turbulence Modeling Resource (TMR); some of the most common cases are the 2D zero pressure gradient flat plate, 2D airfoils, flow over a wall-mounted hump, flow in a diffuser, flow over a backward facing step etc. For the model to be fully validated, it must be in good agreement with numerous validation cases.

Solution verification is focused on how well the governing equations (Navier Stokes) are resolved and code verification is focused on how accurately the model is discretized and implemented in a CFD code. Code verification can be employed by comparing convergence results for the exact same case and settings to other codes with well-defined results. The convergence is defined as the solutions approaching a unique (exact) value as the mesh in the

computational domain is refined. Flow domains are represented using meshes or grids, the most well-defined flow field would be an infinitesimally small grid (a "theoretical" box for every infinitesimal fluid element). If every flow field could be infinitely resolved and solved, then there would be no need for most of the CFD best practices. As the mesh is refined, the computational cost increases, further increasing the computational time. To ensure no bugs have been introduced in coding, a single case is run on systematically refined grids and the same flow characteristic is evaluated across those grids. After a certain refinement, the results should not change significantly. If the results continue to change significantly it suggests additional errors have been introduced by the model or mesh. Solution verification is beyond the scope of this thesis, more information may be found in [8].

2.4 References

[1] White, F., "*Viscous Fluid Flow*," 3rd Edition, McGraw Hill, 2006

[2] Spalart, P. and Allmaras. S., "A One-Equation Turbulence Model for Aerodynamic Flows," AIAA Paper 1992-439, 30th Aerospace Sciences Meeting and Exhibit, Reno, NV, 1992, https://doi.org/10.2514/6.1992-439.

[3] Han, X., Rahman, M. M., and Agarwal, R. K., "Development and Application of a Wall Distance Free Wray-Agarwal Turbulence Model," AIAA Paper 2018-0593, AIAA SciTech Forum, Kissimmee, FL, 8-12 January 2018.

[4] Cakmakcioglu, S.C., Bas, O., Mura, R. and Kaynak, U., "A Revised One-Equation Transitional Model for External Aerodynamics," AIAA Paper 2020-2706, AIAA 2020 Aviation Forum (Virtual), 2020, doi 10.2514/6.2020-2706.

[5] Xue, Y., Tianshu, W., and Agarwal, R., "Development of a New Transition Flow Model Integrating the one-equation Wray-Agarwal Turbulence Model with an Algebraic Intermittency Transport Term," AIAA 2021-2712, July 2021, https://doi.org/10.2514/6.2021-2712

[6] Drikakis, D. and Goldberg, U., "Wall-Distance-Free Turbulence Models Applied to incompressible Flows," International Journal of Computational Fluid Dynamics, Vol. 10, pp 241-243, 1998

[7] Mani, M. and Cary, A., "CFD Verification and Validation for Industrial Applications," 31st Congress of International Council of the Aeronautical Sciences, 2018.

[8] NASA Langley Research Center, Turbulence Modeling Resource Website, 2014, URL https://turbmodels.larc.nasa.gov/naca0012_val.html.

Chapter 3:Validation of the Wray-Agarwal 2017 Turbulence Model for Symmetric NACA Airfoils

3.1 Introduction

The NACA 0012, 0015, and 0018 are symmetric airfoils which are ideal test cases for evaluating the accuracy of different turbulence models due to their simple geometry and availability of experimental data. NASA Turbulence Modeling Resource (TMR) has 2D turbulent flow validation test case for the NACA 0012 airfoil providing pressure distribution, lift, and drag [1]. This validation case serves as an excellent baseline case for evaluations of new turbulence models and CFD codes. In this paper, we consider two turbulence models - The Spalart-Allmaras (SA) one equation turbulence model [2] which has become a very widely used model for computation of aerodynamic flows. The other model considered is the more recently developed Wray-Agarwal (WA) model [3] which has shown improvements over the SA model for many aerodynamic flows. In addition to the computation of flow past NACA 0012 airfoil, SA and WA models are also applied to compute turbulent flows past NACA 0015 and NACA 0018 airfoils at high angles of attack and computed results are compared with the experimental data.

3.2 Mesh Generation and Mesh Independence of Solution Study

Each of the three NACA airfoils was simulated using the same meshing process to ensure consistency. The NACA 0012 airfoil validation case from NASA TMR served as a guideline for the two other test cases. The airfoil was placed at the center of a rectangular domain 500 chord lengths from each boundary to avoid far field point vortex condition. Structured grid was

selected for higher control of inflation layer refinement. ANSYS ICEM software was used to generate a structured grid with O-grid conformity near the airfoil. The grid was generated to ensure y+ << 1 for each airfoil. The first layer height away from the airfoil was $8x10^{-7}$ based on scaled reduction of the minimum wall distance for Reynolds number of $6x10^{6}$. The geometric growth rate was set to maximum 1.2 for all cells in the grid. Present results for the NACA 0012 were calculated on mesh with ≈254,000 hexahedral cells. The NACA 0015 results were calculated with ≈238,000 cells and the NACA 0018 with ≈257,000 cells. Figure 1 shows a typical mesh around NACA 0012 airfoil. The geometry of the airfoils was generated using the explicit equation for 4-digit NACA series airfoils given in Eq. 3 [4].

$$\pm y_t = \frac{t}{0.20}(0.2969\sqrt{x} - 0.1260x - 0.35160x^2 + 0.28430x^3 - 0.10150x^4) \tag{3}$$

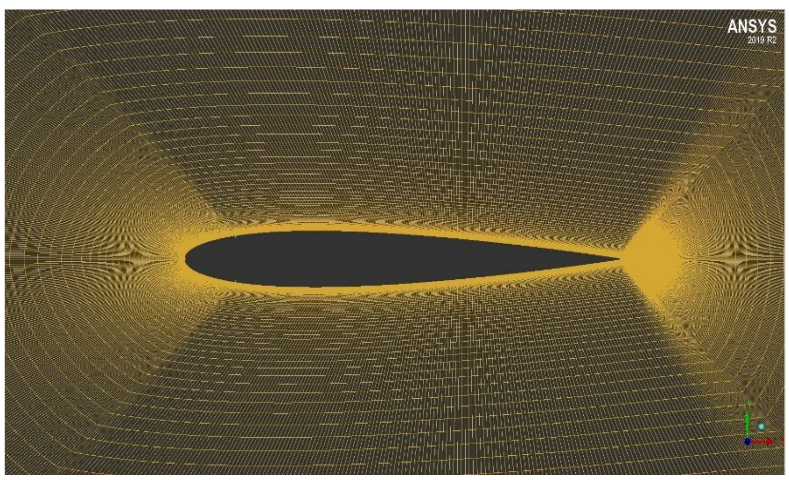

Figure 1: Structured mesh around 2D NACA 0012 airfoil

Tables 1, 2 and 3 show the results of grid independence study for NACA 0012, NACA 0015 and NACA 0018 airfoils. Grid independence was determined using the SA turbulence model.

Table 1: Grid independence study of solution for NACA 0012 airfoil at Reynolds number = 6x10^6 and angle of attack α = 8° using SA model. Error in lift coefficient is calculated against experimental data from Ladson [5].

Mesh	Number of Cells	Error in C_L(%)	Error in C_D(%)
I	~63,000	21.5	220
II	~92,000	0.63	26
III	~153,000	2.12	10.64
IV	~230,000	2.30	9.47
V	~254,000	2.33	9.07
Final (IV)	~230,000	2.30	9.47

Table 2: Grid independence study of solution for NACA 0015 airfoil for Reynolds number = 7x10^5 and angle of attack α = 8°. Error in lift coefficient is calculated against experimental data from Sheldahl & Klimas [6].

Mesh	Number of Cells	Error in C_L (%)	Error in C_D(%)
I	54,000	11.6	84.17
II	101,000	1.73	24.37
III	158,000	1.02	20.87
IV	238,000	0.928	19.39
V	297,000	0.916	19.22
Final (IV)	238,000	0.928	19.39

Table 3: Grid independence study of solution for NACA 0018 airfoil for Reynolds number = 7x10^5 and angle of attack α = 8°. Error in lift coefficient is calculated against experimental data from Sheldahl & Klimas [6].

Mesh Iteration	Number of Cells	C_L Error (%)
I	56,000	1.40
II	162,000	1.15
III	218,000	0.94
IV	257,000	0.89
Final (III)	218,000	0.94

3.3 Results

3.3.1 Comparison of Lift and Drag Coefficients

Computations were performed for the NACA 0012 airfoil at angles of attack from -4.01 to 16.16 degrees using both the WA and SA models. Lift and drag coefficients were computed for

each angle of attack and were compared with the Ladson's [4] tripped data as provided on NASA TMR for fully turbulent flow. To compare the two models with experimental data at different Reynolds numbers, the average error at angles of attack from -4.01 to 16.16 degrees was calculated. Table 4 shows that the average error for SA model was about 3.13% in predicting lift and 9.79% in predicting drag while the average error for WA model was about 0.60% in predicting lift and 20.5% in predicting drag compared to experimental data. Figure 2 shows that the predictions from both models are in good agreement from -4.01 to 10 degrees angle of attack in predicting lift, and from 10.10 to 16. 16 degrees angles of attack, the WA model begins to under predict lift compared to experiment. Figure 2 shows that both the SA and WA models over predict drag coefficient compared to experimental data beyond 6.01 degree angle of attack.

Table 4: Average errors in lift and drag coefficients for NACA 0012 airfoil at Re 6x10^6, Ma = 0.15 for α ranging from -4.01 to 16.16 degrees when compared to experimental data of Ladson [5].

Model	C_L Error (%)	C_D Error (%)
SA	3.13	9.79
WA	0.600	20.5

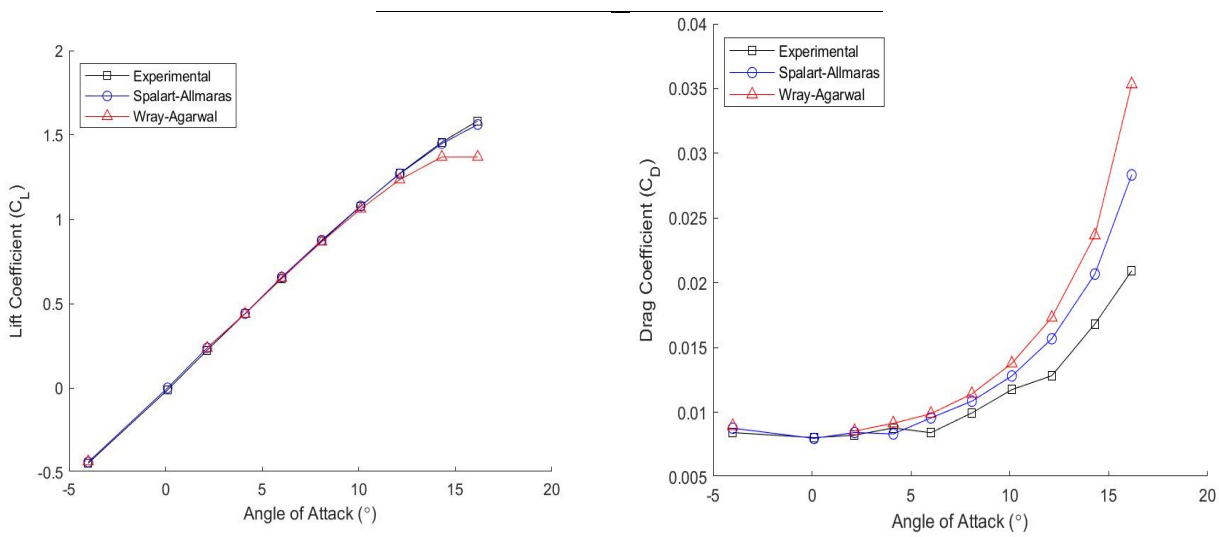

Figure 2: NACA 0012 lift coefficient curves (left) and drag coefficient curves (right) using SA and WA models and their comparison with experimental data of Ladson [5], Re 6x10^6.

After simulations of turbulent flow past NACA 0012 airfoil, computations were performed for turbulent flow past NACA 0015 and 0018 airfoils and were compared with experimental data of Sheldahl and Klima [6] at Reynolds number of $7x10^5$ and Mach of 0.016 for angles of attack from 0 to 14 degrees. The WA model was more accurate in predicting lift coefficient compared to SA model for both NACA 0015 and NACA 0018 airfoils. An error of 40-60 % in prediction of drag coefficient suggests that neither model is suitable for predicting drag. Kekina and Suvanjumrat [7] performed a computational study of turbulent flow past NACA 0015 airfoil using the SA, SST $k - \omega$, and RNG $k - \omega$ models and evaluated the average error for 0 to 10 degrees angle of attack. The lift and drag predictions computed by Kekina and Suvanjumrat were more accurate than the best results of other numerical investigations at that time. Table 5 shows the average error presented by Kekina and Suvanjumrat [7] using the SA model for two different Reynolds number and it is compared here to the average error obtained in the present numerical study using SA and WA model. In the present study, the average error in calculation of drag is high with both models, but still less than the error observed by Kekina and Suvanjumrat. Table 6 compares the average error in simulations for angles of attack from 2 to 14 degrees with experimental data of Sheldahl & Klimas [6] for the NACA 0015 and 0018 airfoils.

Table 5: Average errors in present computations of lift and drag coefficients of NACA 0015 airfoil at Re = $7x10^5$, Ma = 0.03 for α ranging from 0 to 10 degrees and their comparison with computations of Kekina and Suvanjumrat [6].

Computations	Model	C_L Error (%)	C_D Error (%)
Kekina (Re = $1.6x10^5$)	SA	8.01	48.92
Kekina (Re = $3.6x10^5$)	SA	11.18	71.15
Current Study (Re = $7x10^5$)	SA	2.56	39.82
Current Study (Re = $7x10^5$)	WA	3.97	54.69

Table 6: Average errors in present computations of lift and drag coefficients of NACA 0015 airfoil at Re = 7x10^5, Ma = 0.016 for α ranging from 2 to 14 degrees and their comparison with experiments of Sheldahl & Klimas [6].

Airfoil	Model	C_L Error (%)	C_D Error (%)
NACA 0015	SA	9.11	28.81
NACA 0015	WA	7.73	44.80
NACA 0018	SA	8.20	35.43
NACA 0018	WA	7.06	51.18

Figure 3 and Figure 4 show the lift and drag coefficient curves for the NACA 0015 and 0018 airfoils, respectively. Both cases show that the WA model is more accurate in predicting lift for angles of attack greater than 10 degrees. Figures 4 and 5 also show that both models significantly over predict drag. Based on the comparisons presented in Table 5, the drag over prediction was anticipated.

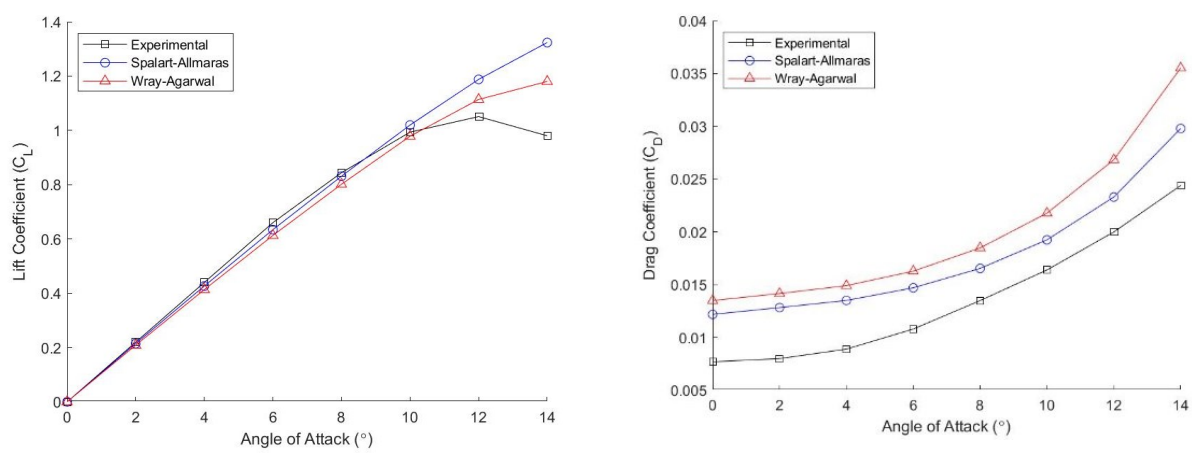

Figure 3: NACA 0015 lift coefficient curve (left) and drag coefficient curve (right) using SA and WA models and their comparison with experimental data of Sheldahl and Klimas [6] at Re = 7x10^5.

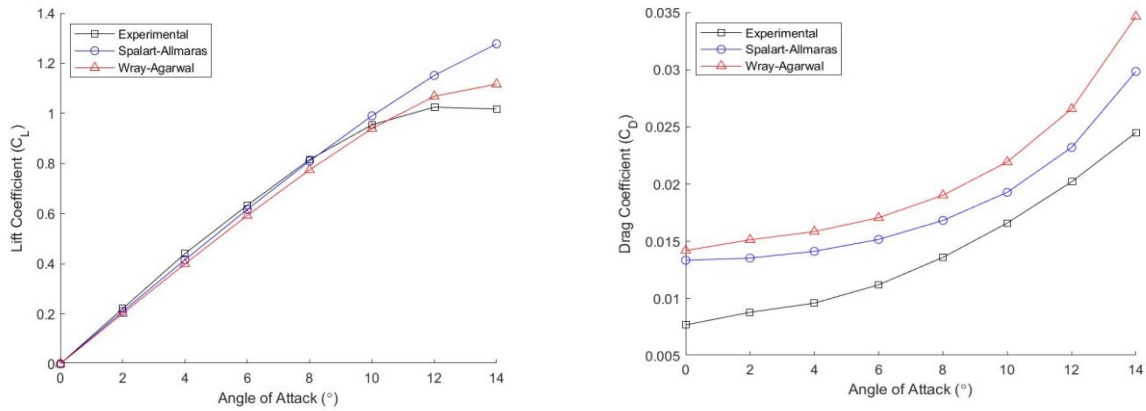

Figure 4: NACA 0018 lift coefficient curves (left) and drag coefficient curves (right) obtained with SA and WA models and their comparison to experimental data of Sheldahl and Klimas [6] at Re = $7x10^5$.

3.3.2 Comparison of Pressure Distributions

In NASA TMR [1], NACA 0012 validation case also compares several data sources for the pressure distribution over the airfoil. NASA TMR suggests comparing the numerical pressure distribution to the data of Gregory and O'Reilly [8] since the leading-edge pressure peak is better resolved. Gregory and O'Reilly performed experiments for turbulent flow past NACA 0012 at Reynolds number of $2.88x10^6$ and Mach number = 0.16. The numerical solution conditions in our simulation were changed to reflect the experimental data case. Figures 5 and 6 show no discernable difference between the pressure distribution calculated with the SA and WA models. Both models were in good agreement with the experimental data for the entire upper surface of the airfoil. Figure 7 shows the WA model is in better agreement for x/c greater than 0.3. Between 0 and 0.3 x/c the SA model tends to over-predict and the WA model tends to under-predict. For all three cases, α = 0, 10, and 15 degrees, both models were in good agreement with experimental data for the NACA 0012 airfoil.

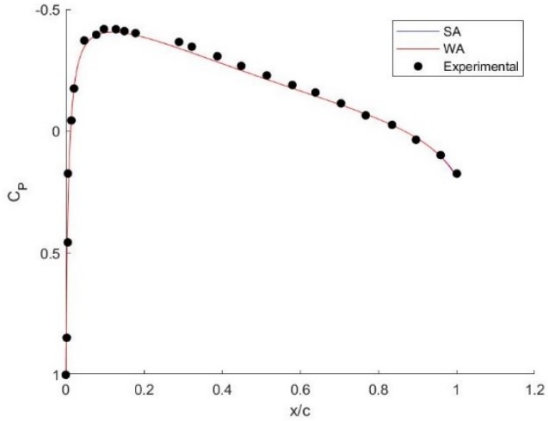

Figure 5: Computed pressure distributions on NACA 0012 airfoil using SA and WA model at α = 0 degree and their comparison with experimental data of with Gregory and O'Reilly [8].

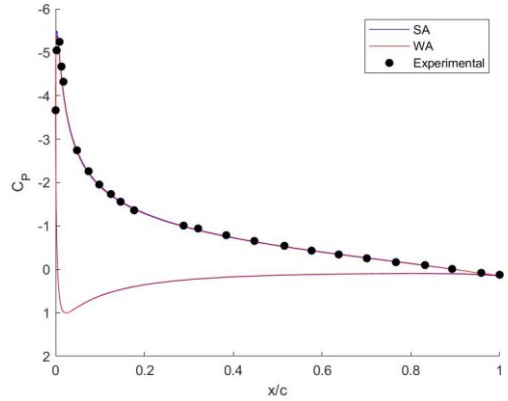

Figure 6: Computed pressure distributions on NACA 0012 airfoil using SA and WA model at α = 10 degree and their comparison with experimental data of with Gregory and O'Reilly [8].

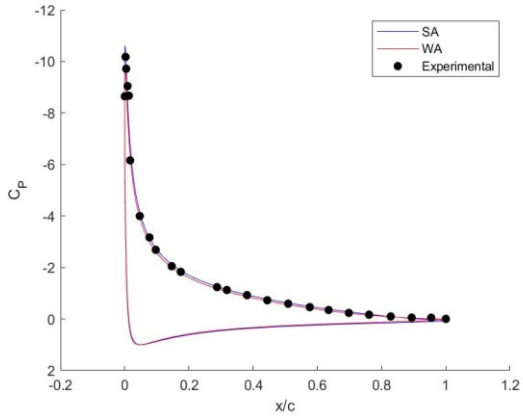

Figure 7: Computed pressure distributions on NACA 0012 airfoil using SA and WA model at α = 15 degree and their comparison with experimental data of with Gregory and O'Reilly [8].

Pressure distributions for the NACA 0015 and 0018 airfoils were computed for Reynolds number = $7x10^5$. Figure 8 shows that both NACA 0015 and NACA 0018 airfoils exhibit the same trends as the NACA 0012 case. There is no notable difference for the 0-degree angle of attack case, and the WA model predicts slightly lower peak pressure for the 6 and 12 degree

cases. Overall, the difference between the models for pressure distribution is insignificant and suggests both models are equivalent in accuracy for similar comparisons.

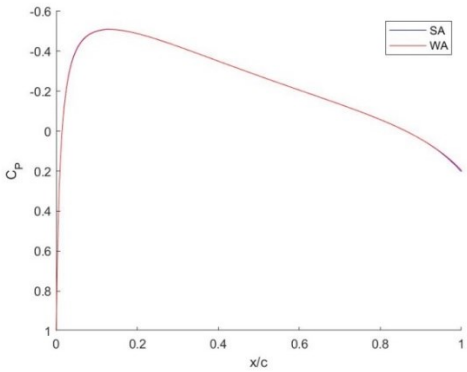

a.) NACA 0015, α = 0 degree

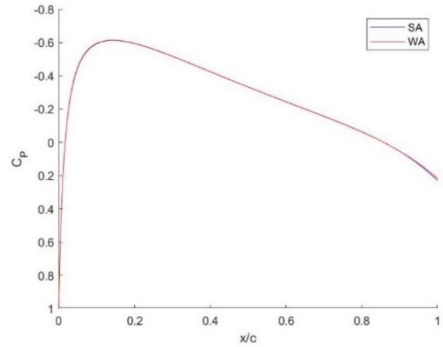

b.) NACA 0018, α = 0 degree

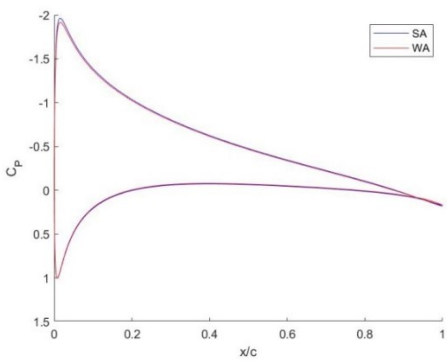

c.) NACA 0015, α = 6 degree

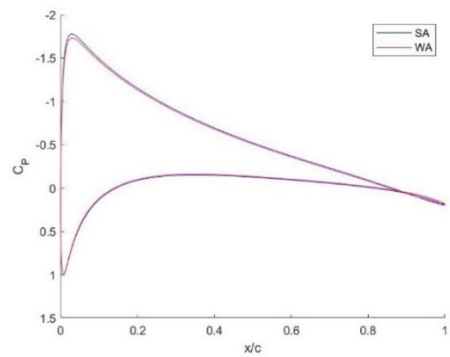

d.) NACA 0018, α = 6 degree

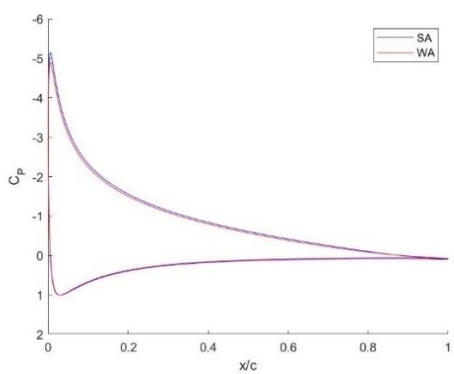

e.) NACA 0015, α = 12 degree

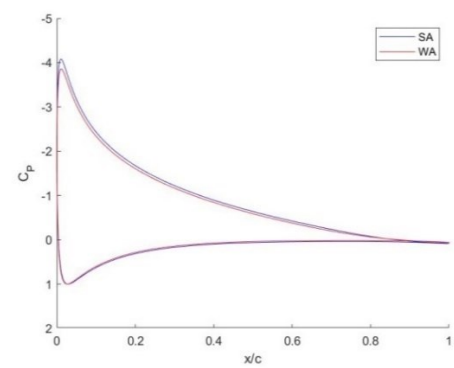

f.) NACA 0018, α = 12 degree

Figure 8: Numerical results for the NACA 0015 and 0018 airfoils at α = 0, 6, 12 degree angle of attack for Reynolds number = $7x10^5$.

3.4 Conclusions

Two one-equation turbulence models, SA, and WA have been applied to simulate 2D turbulent flow over three symmetric airfoils, namely NACA 0012, NACA 0015 and NACA 0018. The numerical results show that the WA model is competitive with SA model and in some cases at higher angles of attack is better than the SA model in accuracy. Further analysis of other airfoil test cases at higher angles of attack including the stall region is necessary to further define the advantages and limitations of WA model compared to SA and other two-equation models.

3.5 References

[1] "2DN00: 2D NACA 0012 Airfoil Validation Case," NASA Langley Research Center Turbulence Modeling Resource Website, 2014, URL https://turbmodels.larc.nasa.gov/naca0012_val.html.

[2] Spalart, P. and Allmaras. S., "A One-Equation Turbulence Model for Aerodynamic Flows," AIAA Paper 1992-439, 30th Aerospace Sciences Meeting and Exhibit, Reno, NV, 1992, https://doi.org/10.2514/6.1992-439.

[3] Han, X., Rahman, M. M., and Agarwal, R. K., "Development and Application of a Wall Distance Free Wray-Agarwal Turbulence Model," AIAA Paper 2018-0593, AIAA SciTech Forum, Kissimmee, FL, 8-12 January 2018.

[4] Jacobs, E., Ward, K., Pinkerton, M., "The Characteristics of 78 Related Airfoil Sections from tests in the Variable-Density Wind Tunnel," NACA Technical Report NACA-TR-460, 1 January 1933.

[5] Ladson, C. L., "Effects of Independent Variation of Mach and Reynolds Numbers on the Low-Speed Aerodynamic Characteristics of the NACA 0012 Airfoil Section," NASA Technical Memorandum 4074, October 1988.

[6] Sheldahl, R. E., and Klimas, P. C., "Aerodynamic Characteristics of Seven Symmetrical Airfoil Sections through 180-degree Angle of Attack for use in Aerodynamic Analysis of Vertical Axis Wind Turbines," Sandia National Laboratories Report, March 1981. https://doi.org/10.2172/6548367.

[7] Kekina, P., and Suvanjumrat, C., "A Comparative Study on Turbulence Models for Simulation of Flow past NACA 0015 Airfoil using OpenFOAM," MATEC Web of Conferences, International Conference on Mechatronics and Mechanical Engineering, 2017, pp. 1–4, https://doi.org/10.1051/matecconf/20179512005.

[8] Gregory, N. and O'Reilly, C. L., "Low-Speed Aerodynamic Characteristics of NACA 0012 Airfoil Section, including the Effects of Upper Surface Roughness Simulating Hoar Frost," Tech. rep., Ministry of Defense: Aeronautical Research Council, 1973.

Chapter 4: Validation of the Wray-Agarwal Algebraic Transition Model for Symmetric NACA Airfoils

4.1 Introduction

Laminar versus turbulent flow on an aerodynamic body significantly impacts drag, lift, and other flow characteristics. An ongoing challenge of computational fluid dynamics (CFD) is increasing the accuracy of simulations while reducing computational cost. Accurate transition location prediction remains a challenging task for Reynolds Averaged Navier Stokes (RANS) solvers. The k-kl-ω transition model requires transport equations for turbulent kinetic energy k, laminar kinetic energy kl and specific dissipation rate ω [1]. SST (Shear Stress Transport) transition model requires three [2] or four [3] transport equations. Nagapetyan and Agarwal [4] developed a transition model which requires only one transport equation for intermittency in addition to the one-equation Wray-Agarwal (WA) turbulence model [5]; it is called the WA-Gamma model. The recently developed Wray-Agarwal Algebraic Transition (WA-AT) model [6] only requires one transport equation (modified WA model equation that includes intermittency γ and an algebraic equation for γ) to model transition. This model has been shown to give accuracy comparable to other higher equation transition models at a much lower computational cost for ERCOFTAC flat plate cases and several 2D flow cases for flow past airfoils. Computation of transitional flows based on Large Eddy Simulation (LES) and Direct Numerical Simulation (DNS) offer better accuracy and overall better resolution of the transitional flow features but are highly compute intensive.

Transition of subsonic flows past aerodynamic bodies is relatively better understood and documented compared to that for transonic and hypersonic flows because the effects of compressibility on transition are not as well understood, and remain an intensive area of research. ERCOFTAC benchmark flat plate cases [7] have been extensively investigated using a variety of transition models because of the simplicity of the geometry and availability of good experimental data. Transition predictions on more complex 2D and 3D bodies have been rather limited due to geometric complexity and limited experimental data. Furthermore, the streamlined bodies common in aerodynamics exhibit a range of transitional Reynolds numbers whereas the flat plate generally exhibits a single value. Note that only smooth bodies without roughness are being considered here. The range of Reynolds numbers introduces higher sensitivity to parameters influencing transition increasing the difficulty of conducting transition experiments on 2D and 3D aerodynamic bodies. Skin friction and flow separation, two large components of aerodynamic drag, are highly dependent on transitional and turbulent flow properties.

The goal of this section is to evaluate the potential of WA-AT model for predicting transition on NACA 0012, NACA 0015, and NACA 0018 airfoils. Computations are also performed using the four equation SST transition model for the purpose of comparison. Transition location, pressure coefficient, skin-friction coefficient, and lift and drag coefficients are computed at various Reynolds numbers.

4.2 Computational Methodology

Commercial CFD solver ANSYS Fluent is employed for solving the RANS equations in conjunction with a transition model. SST transition model is built into Fluent while a UDF is required to implement the WA-AT. CFD-Post and MATLAB are used for post processing and comparing the computations to experimental data. Parametric curves are created using

Solidworks, and the geometry and mesh are generated in ANSYS ICEM. Second-order upwind discretization is used for convection terms in all the equations and the diffusion terns are central-differenced. Solution convergence criterion is based on minimal residual of 10^{-5} for continuity and momentum equations and 10^{-7} for the drag coefficient. If convergence could not be achieved on the proven solution independent mesh, then the next finest mesh is used to achieve convergence. This occurred only once for one angle of attack for the NACA 0015.

4.2.1 Transition Models

The details of SST transition models are not provided here; they are well documented in the literature and the model is built-in ANSYS Fluent. The details of WA-AT model are given below. It should be noted that WA-AT model is based on the wall distance free version of WA model is called WA2018, it is not based on the original WA model (WA2017).

4.2.2 Wray-Agarwal Algebraic Transition (WA-AT) Model

Following the work of Bas and Cakmakcioglu, who included an algebraic transition model in SA model, called SA-BCM, Xue and Agarwal integrated the algebraic intermittency γ term into the WA 2018 model. The WA 2018 model was coupled with the intermittency term through the kinetic energy production term $C_1 RS$ as shown in Eq. (4).

$$\frac{\partial R}{\partial t} + \frac{\partial u_j R}{\partial x_j} = \frac{\partial}{\partial x_j}\left[(\sigma_R R + \nu)\frac{\partial R}{\partial x_j}\right] + C_1 \gamma RS + f_1 C_{2kw}\frac{R}{S}\frac{\partial R}{\partial x_j}\frac{\partial S}{\partial x_j} - (1 - f_1) min\left[C_{2k\epsilon} R^2 \left(\frac{\frac{\partial S}{\partial x_j}\frac{\partial S}{\partial x_j}}{S^2}\right), C_m \frac{\partial R}{\partial x_j}\frac{\partial R}{\partial x_j}\right] \tag{4}$$

For laminar flow, $\gamma = 0$ and for fully turbulent flow, $\gamma = 1$. Eddy viscosity is given by:

$$\nu_t = f_\mu R \tag{5}$$

The gamma equation is given by:

$$\gamma = 1 - exp\left(-\sqrt{Term_1} - \sqrt{Term_2}\right) \tag{6}$$

The $Term_1$ in Eq. (6) defines the transition location, and $Term_2$ assists the intermittency in penetration of the boundary layer.

$$Term_1 = \frac{max(1.2Re_\theta - Re_{\theta c}, 0.0)}{\chi_1 Re_{\theta c}} \tag{7}$$

where

$$Re_\theta = \frac{Re_\nu}{2.193} \text{ and } Re_\nu = \frac{\rho d^2}{\mu}\Omega$$

The variable d is the wall distance. In Eq. (8) below, the local turbulence intensity is different from the work of Menter et al (2) which is calculated by using k and ω. Instead, it is set to a constant value in Eq. (8).

$$Re_{\theta c} = 803.73(Tu_\infty + 0.6067)^{-1.027} \tag{8}$$

Definitions for $Term_2$ and χ_1 and χ_2 are as follows:

$$\begin{aligned} Term_2 &= max\left(\frac{\nu_t}{\nu}\chi_2, 0.0\right) \\ \chi_1 &= 0.02 \\ \chi_2 &= 50 \end{aligned} \tag{9}$$

The boundary conditions for R are:

$$R_\infty = 0.002\nu_\infty\,, \qquad R_{wall} = 0$$

The remaining definitions are consistent with the wall distance free WA 2018 model. The WA model damping function f_μ is designed to account for the wall blocking effect.

$$f_\mu = \frac{\chi^3}{\chi^3 + C_w^3}\,, \qquad \chi = \frac{R}{\nu}$$

where ν is the kinematic viscosity and $R = k/\omega$. The mean strain rate S and the mean vorticity W are given by:

$$S = \sqrt{2S_{ij}S_{ij}}, S_{ij} = \frac{1}{2}\left(\frac{\partial u_i}{\partial x_j} + \frac{\partial u_j}{\partial xi}\right) \tag{10}$$

$$W = \sqrt{2S_{ij}S_{ij}}, W_{ij} = \frac{1}{2}\left(\frac{\partial u_i}{\partial x_j} - \frac{\partial u_j}{\partial xi}\right) \tag{11}$$

The function f_1 is the switching function that triggers the behavior of the one equation $k - \omega$ model near the wall and of one equation $k - \epsilon$ model away from the wall. Switching function f_1 is given by:

$$f_1 = tanh(arg_1^4), arg_1 = \frac{\nu + R}{2}\frac{\eta^2}{C_\mu k\omega} \tag{12}$$

where

$$\begin{aligned} k &= \frac{\nu_T S}{\sqrt{C_\mu}} \\ \omega &= \frac{S}{\sqrt{C_\mu}} \\ \eta &= Smax\left(1, \left|\frac{W}{S}\right|\right) \end{aligned}$$

The model constants are:

$$C_{1k\omega} = 0.0829, \quad C_{1k\varepsilon} = 0.1284$$

$$C_1 = f_1(C_{1k\omega} - C_{1k\varepsilon}) + C_{1k\varepsilon}$$

$$\sigma_{kw} = 0.72, \quad \sigma_{k\varepsilon} = 1.0$$

$$\sigma_R = f_1(\sigma_{k\omega} - \sigma_{k\varepsilon}) + \sigma_{k\varepsilon}$$

$$C_{2k\omega} = \frac{C_{1k\omega}}{\kappa^2} + \sigma_{kw}, \quad C_{2k\varepsilon} = \frac{C_{1k\varepsilon}}{\kappa^2} + \sigma_{k\varepsilon}$$

$$\kappa = 0.41, \quad C_\omega = 8.54$$

$$C_\mu = 0.09, \quad C_m = 8.0$$

4.2.3 Mesh Generation

ANSYS ICEM was used to generate structured meshes for all the three airfoils. The airfoil geometries were generated using a parametric curve in SpaceClaim and were imported into ANSYS ICEM. Domain boundaries were placed 100 chord lengths from the airfoil in all directions. Mesh growth rate was much less than 1.2 and the y^+ value was much less than 1 for all meshes. The meshes generated were 2D meshes in x-y plane of the airfoil which were extruded 1 element in the z-direction. The trailing edge thicknesses were 0.252%, 0.315%, 0.377% for the NACA 0012, 0015, and 0018, airfoils respectively.

4.2.4 Mesh Independence of Solution Study

The NACA 0012, 0015, and 0018 airfoils employ the same meshing process, and the final mesh selected in the simulation has mesh independent solution. A total number of six meshes designated as (ref_0 to ref_5) are generated and evaluated for the NACA 0015 airfoil to

determine the solution dependence of the grid. The simulations are considered converged based on the drag coefficient residual dropping below 10^{-7}. Mesh independence of solution is evaluated for a transitional flow case for flow past NACA 0015 airfoil at Reynolds number of $5 * 10^5$, turbulence intensity of 1%, and turbulent viscosity ratio of 10 at zero angle of attack. Figure 9 shows that the mesh # ref_2 is sufficient for mesh free solution based on minimum change in drag prediction with further mesh refinements. The fourth mesh (mesh # ref_3) has a near wall mesh refinement to provide more resolution for higher angle of attack cases; however it shows little improvement in the solution. The sixth mesh (mesh # ref_5) shows no significant improvement compared to mesh # ref_1, therefor mesh # ref_3 and # ref_5 are not tested for the NACA 0012 and 0018 airfoil convergence studies. Table 7 provides the number of nodes for all six meshes used for all three airfoils. Tables 8, 9 and 10 provide the convergence results for drag coefficient CD on different meshes for the NACA 0012, 0015, and 0018 airfoils, respectively.

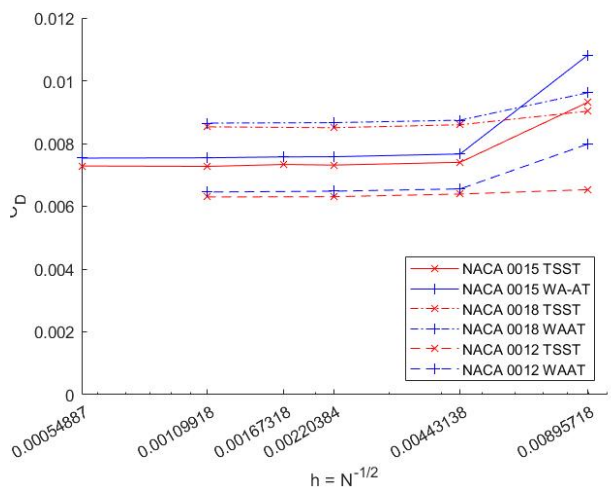

Figure 9: Drag convergence study for the NACA 0012, 0015, and 0018 airfoils at Reynolds number = $5 * 10^5$, turbulence intensity = 1% and viscosity ratio = 10.

Table 7: Mesh node distributions and mesh spacing *h* for six different meshes from coarse to fine.

Mesh	2D Nodes (N)	*h* = N^-1/2
ref_0	12464	0.00895718
ref_1	50924	0.004431377
ref_2	205892	0.002203841
ref_3	357204	0.001673177
ref_4	827684	0.001099177
ref_5	3319364	0.000548874

Table 8: NACA 0012 airfoil: convergence study of drag coefficient C_D at Reynolds number = $5 * 10^5$.

Mesh #	*h*	WA-AT C_D	TSST C_D
ref_0	0.00895718	0.007980585	0.006530674
ref_1	0.004431377	0.006554332	0.006390703
ref_2	0.002203841	0.006481103	0.006305886
ref_4	0.001099177	0.006454464	0.006296567

Table 9: NACA 0015 airfoil: convergence study of drag coefficient CD at Reynolds number = $5*10^5$.

Mesh #	*h*	WA-AT C_D	TSST C_D
ref_0	0.00895718	0.010813	0.0093115734
ref_1	0.004431377	0.007666	0.0073998643
ref_2	0.002203841	0.007578	0.007312
ref_3	0.001673177	0.007574	0.007332
ref_4	0.001099177	0.007546	0.00727
ref_5	0.000548874	0.007536	0.007283836

Table 10: NACA 0018 airfoil: convergence study of drag coefficient C_D at Reynolds number = $5*10^5$.

Mesh #	*h*	WA-AT C_D	TSST C_D
ref_0	0.00895718	0.009618	0.009029
ref_1	0.004431377	0.008743	0.008598
ref_2	0.002203841	0.008665	0.008503
ref_4	0.001099177	0.008651	0.00853

4.2.5 Convergence Criteria

All transitional flow cases were considered converged based on the residuals of continuity and momentum equations dropping below 10^{-5}. In addition, solution convergence was also based on the residual of the drag coefficient over two iterations dropping below 10^{-7}. The drag coefficient convergence of residuals dropping below 10^{-7} was found to ensure that the skin friction and pressure distributions on the airfoil surface did not change with the additional

number of iterations. Transition was determined by evaluation of the skin friction distribution. Figure 10(a) shows an example of skin friction distribution for the NACA 0018 airfoil in the presence of laminar separation bubble. Figure 10(b) shows the skin friction coefficient distribution for the NACA 0015 without a laminar separation bubble. For some cases where laminar separation was present, the transition location was assumed to be the reattachment point indicated in the skin friction distribution. The black arrows in Figure 10 indicate the computed transition location. Cases where laminar separation bubbles were present are noted so that our interpretation of transition location is clear. Accurate resolution of the laminar separation bubble is beyond the scope of this work. In cases where separation bubbles are present, on any given mesh, our goal is to compare the prediction of reattachment/transition location using the WA-AT and TSST model.

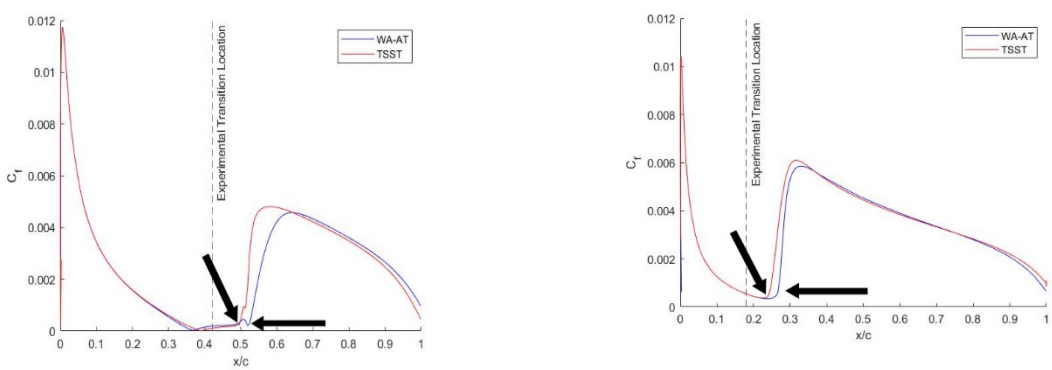

(a) (b)

Figure 10: (a) Computed skin-friction distribution (a) NACA 0018 airfoil, Reynolds number Re = $1 * 10^6$, turbulence intensity Tu = 0.07%, α = 0°, experiment of Timmer 0, (b) NACA 0015, Reynolds number Re = $3 * 10^6$, turbulence intensity Tu = 0.098%, α = 0°, experiment of Baek & Fugslang [11].

4.3 Results

All experimental and numerical data presented in this paper was digitized from the plots using MATLAB grabit. The appendix has detailed tabulated results for the lift, drag, and transition

location computed for the NACA 0012, 0015, and 0018 airfoil cases. The convergence criteria mentioned in the convergence study above was achieved for all the results presented unless otherwise noted; most cases converged beyond minimum convergence criteria. All transition location predictions are for the suction surface of the airfoil.

4.3.1 NACA 0012 Airfoil

The flow past NACA 0012 airfoil has served as a benchmark case for validation of turbulence and transition models due to the availability of large amount of experimental data. Gregory and O'Reilly [12] report the transition location for the NACA 0012 airfoil at Reynolds number = $3.0 * 10^6$. The details of the flow field in the wind tunnel are given, but the turbulence intensity and other flow characteristics are not provided for the transitional flow region. This section also compares the present results to the numerical results of Yousefi and Razeghi [13], who investigated the transitional flow over NACA 0012, 0015 and 0018 airfoils using CFD FORTRAN code and a vorticity panel method combined with the integral momentum and kinetic energy shape parameter equations to represent the viscous region. Yousefi and Razeghi used the e^N method for transition and provided no flow characteristics other than the Reynolds number of the flow. The calibration of the transitional $k - \omega - \gamma - Re_{\theta t}$ (TSST) model by Barroulliet et al. [14] compared their computations to the experiment of Gregory and O'Reilly [12]. Barroulliet et al. [14] used a turbulence intensity of 0.3% and a viscosity ratio of 100 for the calibration case and employed FANSC, a finite volume structured code. The results of Barroulliet et al. showed better agreement with the experimental data for transition location prediction employing the TSST model for the NACA 0012 airfoil over all angles of attack compared to the present results using TSST model in Fluent. This difference in the results is likely due to how the turbulent viscosity ratio is defined in ANSYS Fluent. The ANSYS Fluent user guide suggests a turbulent

viscosity ratio between 1 and 10 for external flows, but a value of 100 may be sensible for internal flows [15]. Table 11 shows the effect of turbulent viscosity ratio on the predictions of TSST transition model. This case was also computed by Nitya and Ranjan using ANSYS Fluent and they showed much better agreement with experiment using the TSST model [16] compared to the present results. Nitya and Ranjan did not state the turbulent viscosity ratio and turbulent intensity used in their implementation of the TSST model; therefore, it is hard to determine the difference between their computations and present results.

Table 11: Effect of turbulent viscosity ratio μt/μ on flow characteristics for the Transition SST (TSST) model at Reynolds number Re = $3*10^6$, turbulence intensity Tu = 0.3%, α = 0°.

μ_t/μ	C_L	C_D	Transition Location (x/c)	Experimental Location [12]
10	1.56E-06	0.004281	0.66	
100	-9.01E-07	0.00471963	0.6	~ 0.45
1000	1.81E-06	0.005057	0.55	

Although better predictions using the TSST model have been reported against the experimental data of Gregory and O'Reilly [12] for NACA 0012 airfoil, the predictions from WA-AT model presented here are sufficient to show its value. The objective of this chapter is to demonstrate that the WA-AT model is accurate in prediction of transition location. The computations using the TSST model are provided for the purpose of comparison between the two models. It should be noted that TSST model is a part of the suite of turbulence/transition models in Fluent while WA-AT is implemented as UDF. Since the WA-AT model has a single transport equation and still has accuracy comparable to the TSST model, this demonstrates its great potential in predicting transition accurately with high computational efficiency.

Figure 11 shows that the WA-AT model is in good agreement with the experimental transition location at all angles of attack. Table A1 in the Appendix provides the tabulated results

at all angles of attack for Re = $3 * 10^6$. The TSST model predicts delayed transition from zero to five degree angles of attack and beyond five degree angle of attack, the TSST model agrees well with the experimental data. Figure 12 shows that both TSST and WA-AT models are in good agreement for the lift coefficient prediction.

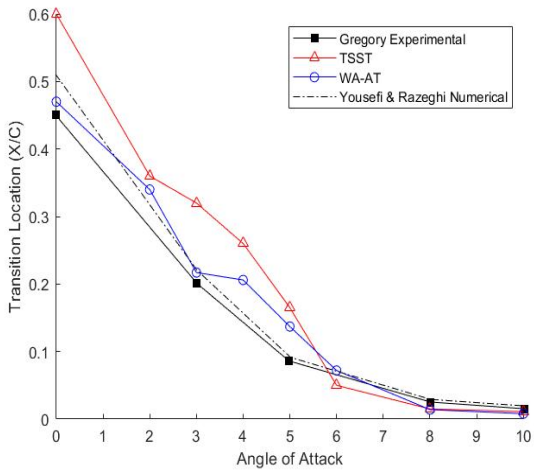

Figure 11: Computed transition location vs. angle of attack using the WA-AT and TSST models at Reynolds number Re = $3*10^6$, turbulence intensity Tu = 0.3% and μ_t/μ = 100 compared to experiment of Gregory and O'Reilly [12].

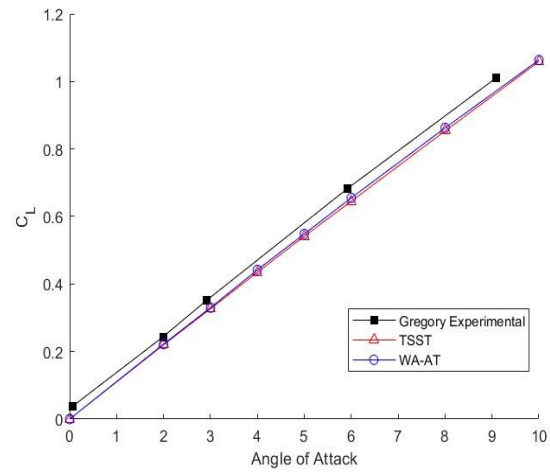

Figure 12: Computed lift coefficient vs. angle of attack using the TSST and WA-AT models at Reynolds number Re = $3*10^6$, turbulence intensity Tu = 0.3% and μ_t/μ = 100 compared to experiment of Gregory and O'Reilly [12].

Figure 13 shows the drag coefficient prediction using both TSST and WA-AT models compared to the experimental results of Gregory and O'Reilly [12]; it shows that the WA-AT model is in better agreement with the experimental data compared to the TSST model. The delay in transition onset prediction corresponds to the under-prediction of drag by the TSST model. Figure 14 shows the drag polar for both the models and includes the numerical results of Barrioullet et al. [14], who achieved much better agreement for transition location using the TSST model in the FANSC code with the same parameters for μ_t/μ and Tu. The WA-AT model still gives a closer prediction than Barrioullet et al. [14] and only requires the turbulence intensity Tu as input.

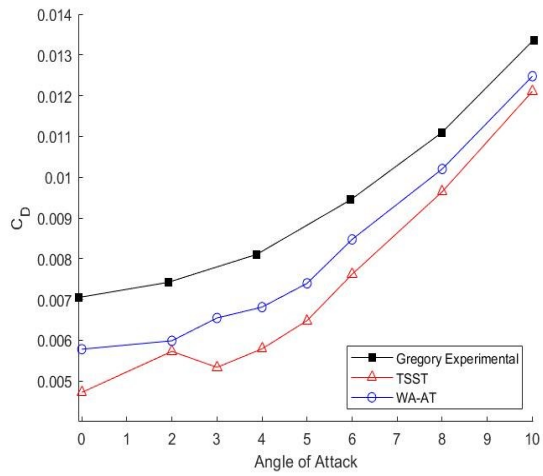

Figure 13: Comparison of drag coefficient prediction using the TSST and WA-AT model with experiment of Gregory and O'Reilly [12], Re = $3*10^6$.

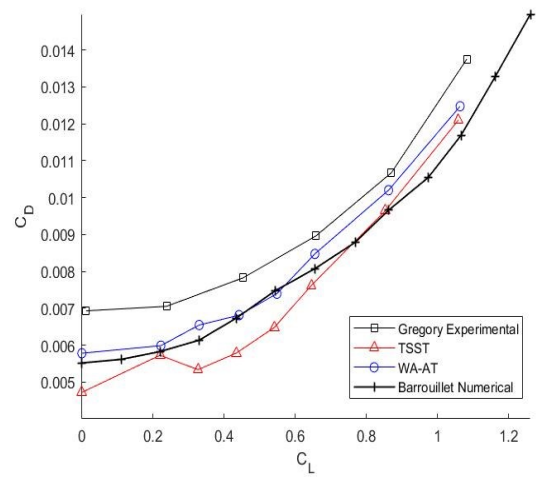

Figure 14: Drag polar comparison using the WA-AT and TSST model with results of Barroullet et al. [14] and experiment of Gregory and O'Reilly [12], Re = $3*10^6$.

Figure 15 shows that both the WA-AT and TSST model predict nearly identical pressure distributions. Both models agree with the experimental data for the six degree angle of attack case extremely well. There is slight difference in the suction peak pressure at zero degree angle of attack; it is likely due to the digitization of data from the scanned plot. Overall, both models predict the same pressure distribution in good agreement with the experimental data.

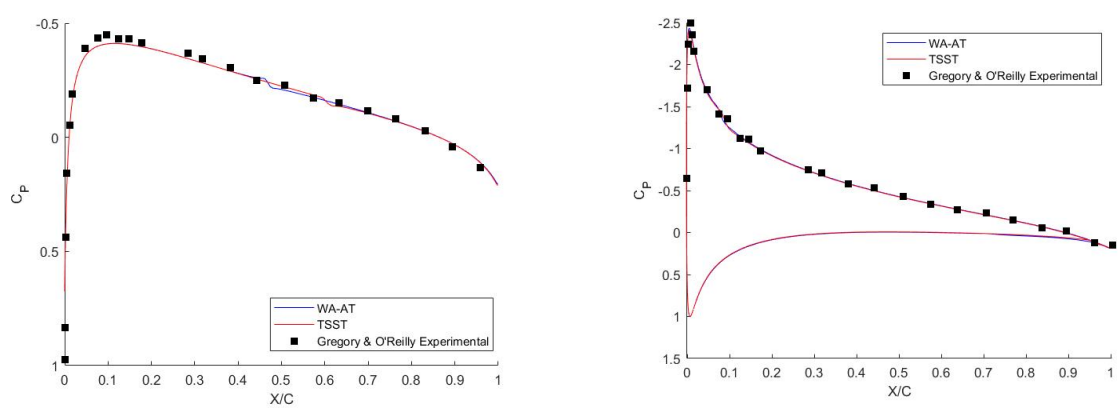

(a.) $\alpha = 0°$ (b.) $\alpha = 6°$

Figure 15: Comparison of pressure coefficient distribution using the WA-AT and TSST model with the experimental data of Gregory and O'Reilly [12], Reynolds number Re = 3*10^6, turbulence intensity Tu = 0.3% and $\mu_t/\mu = 100$.

4.3.2 NACA 0015 Airfoil

Present computations are compared to the experimental results of Baek & Fugslang [11], and the numerical results of Yousefi & Razeghi [13]. Yousefi and Razeghi utilized the vortex panel/integral boundary layer method in combination with an e^N transition model to predict the transition flow characteristics of the NACA 0012, 0015, and 0018 airfoils. The transition location predictions are compared for Reynolds number = $3 * 10^6$ with a turbulence intensity Tu = 0.098%, and for a Reynolds number = $6 * 10^6$ with a turbulence intensity = 0.108% in Mach 0.3 freestream flow. Figure 16 shows that the WA-AT model predicts the transition location better than the TSST model for angles of attack from 0 to 10 degree. Between 0 and 6 degree angles of attack, the WA-AT results are significantly closer to the experimental transition location, and beyond 6 degree angle of attack both models are comparable in accuracy in prediction of transition location. Figure 17 shows the comparisons for Re = $6 * 10^6$ case, where the TSST model captures the trend in transition shift better than the WA-AT model. Figure 16 however does show that the WA-AT model prediction is similar to the calculation of Yousefi and Razeghi [13]. A viscosity ratio of 10 is assumed in all computations. Table A2 in the Appendix provides the tabulated results at all angles of attack for Re = $3 * 10^6$ and Table A3 in the Appendix provides the tabulated results at all angles of attack for Re = $6 * 10^6$.

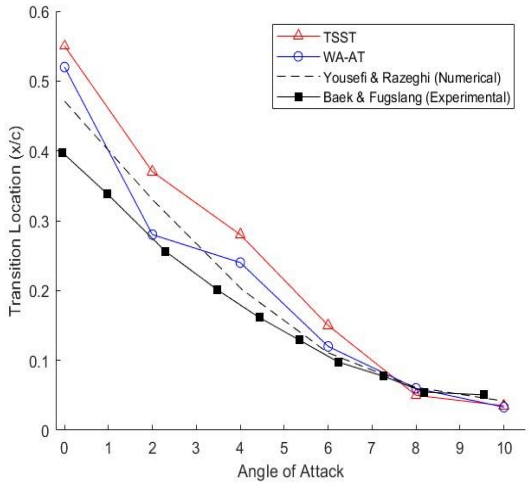

Figure 16: Comparison of transition location predictions using WA-AT and TSST model with the numerical results of Yousefi & Razeghi [13] and the experimental results of Baek and Fugslang [11], Re = $3*10^6$, Tu= 0.098%.

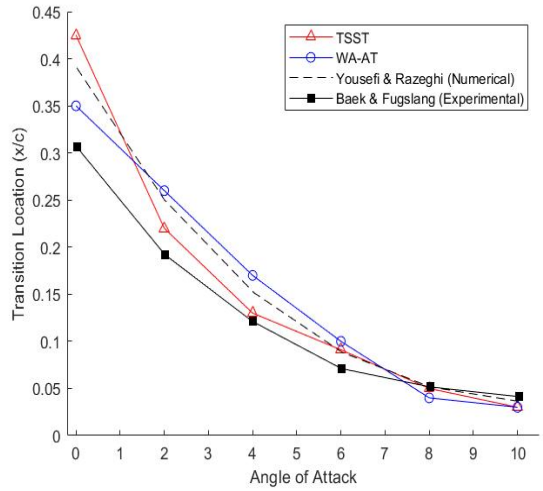

Figure 17: Comparison of transition location predictions using WA-AT and TSST model with the numerical results of Yousefi & Razeghi [13] and the experimental results of Baek and Fugslang [11], Re = $6*10^6$, Tu= 0.108%.

Transition was characterized by the sudden increase in skin friction as described in the convergence criteria section above. Figure 18 (a) shows the skin friction distribution for the zero degree angle of attack case, and Figure 18 (b) shows the skin friction distribution for the six degree angle of attack case at case at Re = $3*10^6$. The trends in skin-friction predicted by the two models are very similar, the only difference being the location of the transition and the peak magnitude of the skin friction coefficient. The magnitude of the skin friction is also dependent on the location of transition.

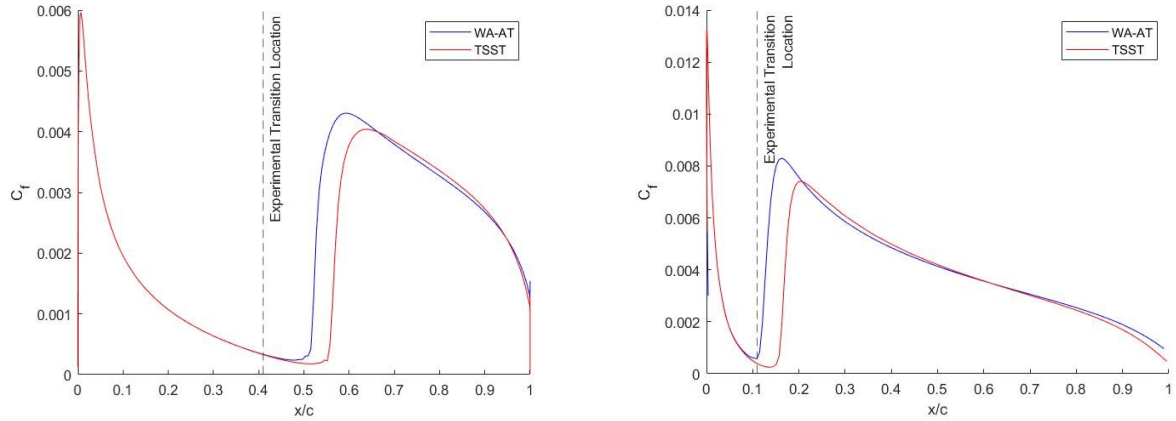

(a) Zero degree AOA **(b) Six degree AOA**

Figure 18: Skin friction distribution on the NACA 0015 airfoil at Re = 3*10^6 and (a) α = 0º and (b) α = 6º; experimental transition location is from Baek & Fugslang [11].

The turbulent viscosity ratio for the TSST simulation cases was varied to show its effect on the transition location. Figure 19 shows the effects of low, medium, and high viscosity ratio on transition location prediction.

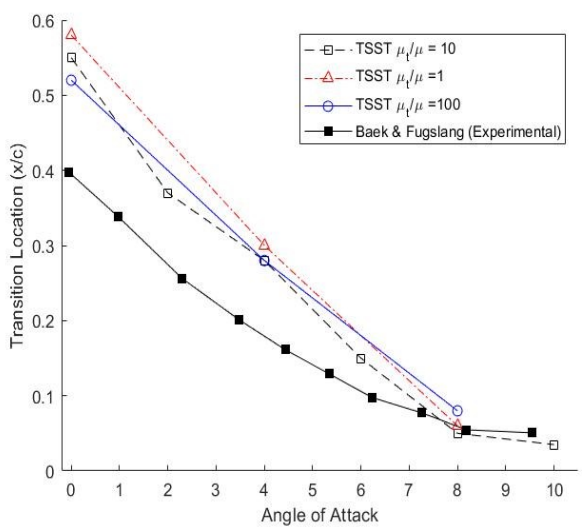

Figure 19: Transition location predictions using the TSST model for turbulent viscosity ratio (μ_T/μ) = 1, 10, and 100; Re = $3*10^6$, Turbulence intensity Tu = 0.098%.

4.4 NACA 0018 Airfoil

Laminar separation bubbles (LSB) were predicted for most angles of attack by both the WA-AT and TSST models. Figure 20 shows the transition location prediction based on the assumed transition at the re-attachment location of the bubble. The WA-AT and TSST model predict similar delayed transition locations below six degree angle of attack. Beyond six degree angle of attack, the WA-AT model predictions are close to the results of Yousefi & Razeghi [13] and are in good agreement with the experimental data. Figure 21 shows the lift coefficient predictions compared to the experimental results of Timmer [10]. Both models predict identical results below six degree angle of attack and agree well with the experimental data. Beyond six degree angle of attack, the TSST model continues to agree well with the experimental data whereas the WA-AT model begins to slightly over-predict the lift. Table A4 in the Appendix provides the tabulated results at all angles of attack for Re = $1*10^6$. The presence of laminar separation bubbles makes the comparison of experimental and numerical results difficult. LSB resolution is highly dependent on the grid resolution and numerical dissipation. In addition, how the models predict the shear stresses may influence the size/length of the laminar separation bubbles. This comparison does show similar LSB termination distances for a given mesh resolution between the two models.

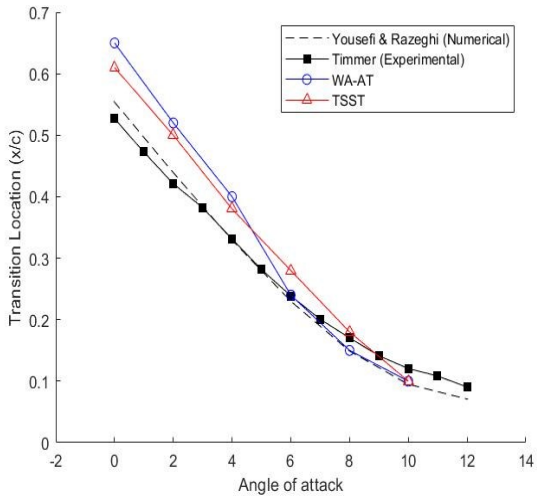

Figure 20: Comparison of transition location on NACA 0018 airfoil at Re $= 1 * 10^6$ and turbulence intensity Tu = 0.07% using TSST and WA-AT model with numerical results of Yousefi & Razeghi [13]and experimental data of Timmer [10].

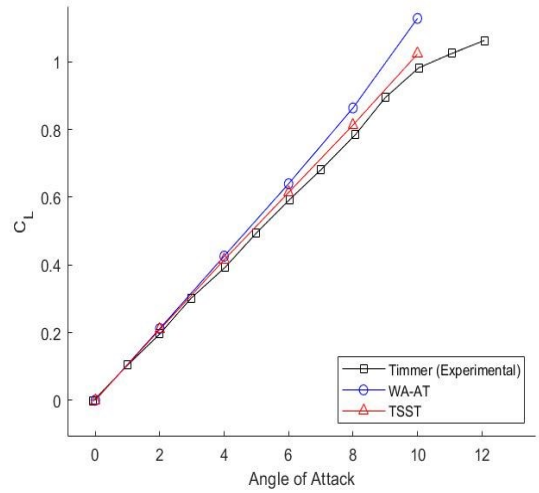

Figure 21: Comparison of lift coefficient of NACA 0018 airfoil at Re $= 1 * 10^6$ and turbulence intensity Tu = 0.07% using TSST and WA-AT model with experimental data of Timmer [10].

4.5 Conclusions

The NACA 0012, 0015, and 0018 airfoils serve as commonly used benchmark validation test cases for determining the accuracy of turbulent /transitional models used with RANS equations. This investigation has demonstrated that the recently developed one-equation transition model - the WA-AT is comparable in accuracy to the four equation TSST model for computing the transitional flow over NACA 0012 and 0015 airfoils. The implementation of the WA-AT model is easier since it only requires the specification of inflow turbulence intensity and not the turbulent viscosity ratio required by higher equation transition models including the four equation TSST model.

The simulation of transitional flow over NACA 0012 showed that the results from WA-AT model agree well with the experimental data and showed improvement over the TSST implementation presented by Barroulliet et al. [14]. Both WA-AT and TSST models agree quite

well in the prediction of the distribution of the pressure coefficient on NACA 0012 airfoil compared to experimental data. The lift coefficient predictions using the two models were identical at all angles of attack and the WA-AT model predicted the drag coefficient more accurately than the TSST model. The TSST calibration test case was implemented in FANSC code by Barrouillet et al. [14] and used the same parameters for turbulent intensity and viscosity ratio that were used in the present implementation of WA-AT in Fluent using a UDF. The calibration case showed excellent results in prediction of transition location and for the lift coefficient using the TSST model compared to experimental data; however, the WA-AT model outperformed the TSST model in the prediction of drag polar compared to the TSST model.

The NACA 0015 airfoil validation case also showed the WA-AT model performing better than the TSST model for Re = $3*10^6$, and the TSST model overall performing better for Re = $6*10^6$ case. Beyond eight degree angle of attack, both the WA-AT and TSST model agree will with the experimental data as well as the numerical results of Yousefi and Razeghi [13] at both Reynolds numbers. The results for skin friction distribution also showed nearly identical trends using both models, the only difference being in the location at which the skin friction increases.

For the NACA 0018 validation case, limited results are presented due to the presence of laminar separation bubbles at all angles of attack. The accurate resolution of laminar separation bubble is highly dependent on the mesh quality and numerical dissipation. This test case did point out the similarities in the prediction of the separation bubble termination location by the two models. The TSST model was found to be more accurate in predicting the lift coefficient and the WA-AT model over-predicted the lift coefficient at higher angles of attack.

In summary, the WA-AT model is much easier to implement than the TSST model and offers similar accuracy for the transitional flow predictions for the airfoils considered. The WA-AT model demonstrates the correct trend in variation of the transition location with angle of attack and Reynolds number. As the angle of attack of an airfoil increases, the transition location shifts toward the leading edge. The increase in Reynolds number also shows shift of the transition location toward the leading edge. The advantage of the WA-AT model is the reduction in number of transport equations to only one for simulating transitional flow using the RANS equations. This validation study shows that the WA-AT model is comparable in accuracy to the TSST model but with much higher computational efficiency being a one equation model.

4.6 References

[1] Walters D. K. and Cokljat D., "A Three-Equation Eddy-Viscosity Model for Reynolds-Averaged Navier-Stokes Simulations of Transitional Flow," ASME Journal of Fluids Engineering, Vol. 130, No. 12, 2008, p. 121401, doi:10.1115/1.2979230.

[2] Menter, F. R., Langtry, R. B., Likki, S. R., Suzen, Y. B., Huang, S., and Völker, P. G., "A Correlation-Based Transition Model Using Local Variables --- Part I: Model Formulation," ASME J. of Turbomachinery, Vol. 128, No. 3, 2004, pp 413-422.

[3] Menter, F. R., Smirnov, P. E., Liu, T., and Avancha, R., "A One-Equation Local Correlation-Based Transition Model," Flow, Turbulence and Combustion, Vol. 95, 2015, pp. 583–619.

[4] Nagapetyan, H., and Agarwal, R. K., "Development of a New Transitional Flow Model Integrating the Wray-Agarwal Turbulence Model with an Intermittency Transport Equation," AIAA Paper 2018-3384, AIAA 2018 Fluid Dynamics Conference, Atlanta, Georgia, 25-29 June 2018.

[5] Han, X., Wray, T. J., and Agarwal, R. K., "Application of a New DES Model Based on Wray-Agarwal Turbulence Model for Simulation of Wall-Bounded Flows with Separation," AIAA Paper 2017-3966, June 2017, doi:10.2514/6.2017-3966.

[6] Xue, Y., Wen, T., and Agarwal, R. K., "Development of a New Transitional Flow Model Integrating the One Equation Wray-Agarwal Turbulence Model with an Algebraic Intermittency Transport Term," AIAA Paper 2021-2712, AIAA Aviation 2021 Forum (Virtual), 2021, doi:10.2514/6.2021-2712.

[7] ERCOFTAC (European Research Community on Flow, Turbulence and Combustion), http://ercoftac.mech.surrey.ac.uk/ [retrieved 20 June 2021]

[8] Han, X., Rahman, M.M., and Agarwal, R.K., "Wall-Distance Free Wray-Agarwal Turbulence Model with Elliptic Blending," AIAA Paper 2018-4044, 2018 AIAA Fluid Dynamics Conference, Atlanta, GA, 25-29 June 2018.

[9] Cakmakcioglu, S.C., Bas, O., Mura, R., and Kaynak, U., "A Revised One-Equation Transitional Model for External Aerodynamics," AIAA Paper 2020-2706, AIAA Aviation Forum (Virtual), 2020, doi 10.2514/6.2020-2706.

[10] Timmer, W. A., "Two-Dimensional Low-Reynolds Number Wind Tunnel Results for Airfoil NACA 0018," Wind Engineering, Vol. 32, No. 6, 2008, pp. 525-537.

[11] Baek, P. and Fuglsang, P., "Experimental Detection of Transition on Wind Turbine Airfoils," Proceedings of European Wind Energy Conference, Marseille, France, 2009.

[12] Gregory, N. and O'Reilly, C. L., "Low-Speed Aerodynamic Characteristics of NACA 0012 Aerofoil Section Including the Effects of Upper-Surface Roughness Simulating Hoar Frost," Ministry of Defense, A. R. C. R. & M. No. 3726, London, 1973.

[13] Yousefi, K. and Razeghi, A., "Determination of the Critical Reynolds Number for Flow over Symmetric NACA Airfoils," AIAA SciTech Forum, 2018, doi: 10.2514/6.2018-0818.

[14] Barrouillet, B., Laurendeau, E., and Yang, H., "Calibration of the Transitional $k-\omega-\gamma-Re_{\theta t}$ Turbulence Model," AIAA Journal, Vol 60, No. 7, July 2022, doi.org/10.2514/1.J060696.

[15] "Ansys Fluent User's Guide 19.2," ANSYS INC, 2018.

[16] Nitya, M. and Ranjan, R., "Numerical Investigation of Transitional Flows over NACA 0012 Airfoil," Fluid Mechanics and Fluid Power (FMFP) Conference, RJ, India, 2021.

[17] Rooij, R.V., "Modification of the Boundary Layer Calculation in RFOIL for Improved Airfoil Stall Prediction," Delft University of Technology, Report IW-96087R, Netherlands, 1996.

[18] Wynnychuk, D. and Yarusevych, S., "Characterization of Laminar Separation Bubbles Using Infrared Thermography," AIAA Journal, Vol. 58, July 2020, doi.org/10.2514/1.J059160.

Chapter 5:Application of the Wray-Agarwal Turbulence Model for Flow past Joukowski Airfoil: High Fidelity CFD Workshop 2022 Verification Case

5.1 Introduction

The Joukowski airfoil has been selected as a benchmark validation and verification test case by the High-Fidelity Computational Fluid Dynamics (HiFiCFD) Workshop 2022 [1]. The stated goal has been to test the convergence behavior of different turbulence models in different CFD solvers with particular emphasis on SA-[neg]-QCR 2000 [1] turbulence model. This paper studies the accuracy and convergence behavior of Wray-Agarwal (WA) [2] and standard Spalart-Allmaras (SA) [3] one equation turbulence models by computing the flow past Joukowski airfoil on a sequence of workshop specified grids from coarse to fine [1]. The benchmark case has free stream Mach number M = 0.15, chord Reynolds number Re = $6x10^6$ and angle of attack of 0 degrees. The goal is to evaluate the convergence of drag coefficient on a sequence of seven grids using WA 2017 model and original version of SA model in ANSYS Fluent. The primary focus of this study is to obtain mesh independent solutions of drag coefficients using the WA and standard SA turbulence model and compare their convergence rates on seven grids from grid # 0 to grid # 6. The results are quantitively compared with those reported by Diskin et al [4] for SA-neg-QCR2000. The WA model is implemented in ANSYS Fluent as a UDF; therefore comparison of computational work units is not presented since the SA model is a built-in part of the Fluent. However, the convergence behavior of WA model similar to or better than the SA

model demonstrates that the UDF does not introduce any additional numerical errors and also the UDF implementation of WA model in ANSYS Fluent is correct.

The HiFiCFD workshop for the Joukowski airfoil provided the meshes and boundary conditions. The requirements of the workshop for the SA-neg-QCR-2000 were applied to obtain the required results for SA and WA models in ANSYS Fluent. The procedure presented in the workshop has been mimicked in this paper except where noted. Mandatory objective 1 and monitoring of the L^2-norm of the density residual for free stream Mach number M = 0.5 were not evaluated in this paper.

5.2 Computational Methodology

5.2.1 Mesh Generation

Galbraith [1] has provided a series of meshes for the Joukowski airfoil prescribed by High Fidelity CFD Workshop 2022 to the workshop participants. The python script provided was used to generate the airfoil and boundaries which were then imported to ANSYS ICEM. The meshes were then extruded 1 element in the Z direction, normal to the airfoil plane. A family of seven grids was used in ANSYS Fluent, numbered 0 to 6 from coarse to fine. The finest mesh, grid # six, was used to calculate the “truth” drag coefficient as instructed in the HiFi CFD Workshop 2022. More information regarding the python script may be found on the NASA TMR website for High-Fidelity CFD Workshop 2022 [5]. Figure 22(a) shows the Joukowski airfoil geometry, and Fig. 22(b) shows the computational domain with boundaries generated by Galbraith’s code [1].

(a) Joukowski airfoil geometry

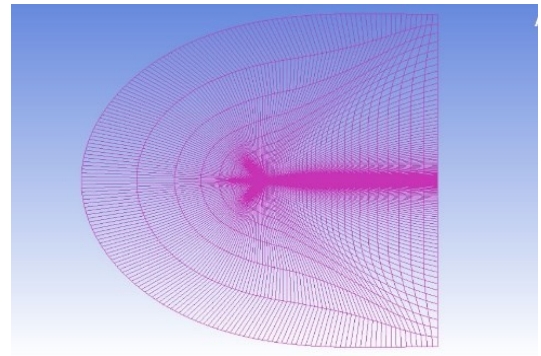

(b) Computational domain for grid # 1

Figure 22: Joukowski airfoil geometry and grid # 1 using boundary conditions from [1].

5.2.2 Flow Conditions

The HiFiCFD 2022 workshop suggests solving the compressible Reynold-Averaged Navier-Stokes equations at a free stream Mach number of 0.15, Reynolds number of $6 * 10^6$ and the angle of attack of 0° [1]. This investigation uses the freestream Mach number = 0.15, Reynolds number = $3 * 10^6$, and angle of attack = 0°. A heat capacity ratio $\gamma = 1.4$, Prandtl number $Pr = 0.72$, and turbulent Prandtl number $Pr_t = 0.9$ are used to match the workshop recommendations. The dynamic viscosity is determined by Sutherland's law with reference values of $\mu_0 = 1.716 * 10^{-5}\ kg/(ms)$, $T_0 = 491.6R$ and $S = 198.6\ R$. Sutherland's law is given in Eq. (13).

$$\mu(T) = \mu_0 \left(\frac{T}{T_0}\right)^{3/2} \left(\frac{T_0 + S}{T + S}\right) \tag{13}$$

5.3 Results

The computations utilize a pressure-based solver with pressure velocity coupling in ANSYS Fluent. Reynolds number = $3 * 10^6$ is used instead of suggested Reynolds number = $6 * 10^6$ but the free stream Mach number, 0.15, is the same. A small change in the Reynolds number may slightly affect the magnitude of the predicted drag but it should not affect the overall

convergence trends for comparison. The remaining boundary conditions match the conditions given in [1]. The convergence criterion is based on the drag coefficient calculation with minimum residual of 10^{-7} in addition to continuity and momentum equations convergence dropping below 10^{-5}. The solution method utilizes Green-Gauss cell-based method for the velocity gradients, and a linear scheme for pressure. Total, viscous and pressure drag are computed on every mesh. A family of seven meshes, labeled zero to six, is used to compare the computations from SA and WA model, the meshes for the airfoil were provided by Galbraith [1] for the workshop. The finest mesh, mesh # 6, is used to calculate the "truth" value for the error comparison. As a result, the drag prediction plots have seven points and the error convergence plots have six points. A linear best fit line is calculated for the error convergence plots to help evaluate the slope of the convergence. If the R^2 value was below 0.99, the linear line was plotted in addition to the error convergence lines. All convergence plots show the reference second order and third order convergence lines provided by Galbraith [1]. The expected convergence rate is determined by the polynomial of degree P of the discretization methods used. Optimal convergence rates for non-adjoint solvers are typically of order P+1. If the convergence rate of the Wray-Agarwal model matches the convergence rate of the Spalart-Allmaras model in ANSYS Fluent it suggests that the UDF implementation of WA model in Fluent is not introducing any additional error.

5.3.1 First-Order Solution on Hexahedral Meshes

The first order upwind scheme was used for convection terms in momentum, energy, and turbulent viscosity equations. Table 12 shows the convergence results for the drag coefficient on the hexahedral mesh. N is defined as the number of 2D nodal points and h describes the nominal mesh spacing. Both models show some reduction in the viscous drag coefficient with mesh

refinement. A more significant reduction with respect to mesh refinement is seen for the pressure drag coefficient. The pressure drag coefficient follows a similar convergence trend as the total drag coefficient. The total drag coefficient is the sum of the viscous and pressure drag coefficients. The "truth" coefficients are predicted from grid # 6.

Table 12: Convergence of total, pressure and viscous drag coefficients for first-order solution on grid #0 to grid #6.

Model	Grid #	N	$h = N^{-1/2}$	C_D	C_{Dp}	C_{Dv}
	0	864	0.034021	0.090118652	0.082303997	0.007814655
	1	3264	0.017504	0.051860913	0.044337591	0.007523322
	2	12480	0.008951	0.029533326	0.022129304	0.007404022
SA	3	49536	0.004493	0.019022843	0.011611008	0.007411835
	4	197376	0.002251	0.013938179	0.006524572	0.007413607
	5	787968	0.001127	0.011372262	0.00393767	0.007434592
	6	3148800	0.000564	0.010113478	0.002674549	0.007438929
	0	864	0.034021	0.091713771	0.08255962	0.009154151
	1	3264	0.017504	0.053424512	0.044591794	0.008832718
	2	12480	0.008951	0.03074766	0.022322737	0.008424923
WA	3	49536	0.004493	0.019469622	0.01171207	0.007757552
	4	197376	0.002251	0.014250824	0.006567542	0.007683282
	5	787968	0.001127	0.011676205	0.004014652	0.007661553
	6	3148800	0.000564	0.010385211	0.002740347	0.007644865

As shown in Table 12, the total drag coefficient approaches the "truth" value of drag coefficient as the mesh becomes finer. Figure 23 shows the drag convergence curves for WA and SA model as the mesh becomes finer. Both models exhibit the same convergence trends for the drag coefficient with convergence rate of approximately 1.2. The error was calculated using the relative error based on the "truth" value. Figure 23(a) shows that the convergence behavior for the total drag using the two models is nearly identical. The only difference in Fig. 23(a) is in the magnitude of the result; the WA total drag prediction is slightly higher than that predicted by the SA model. Figure 23(b) shows both the WA and SA model exhibiting similar convergence trends almost of first order. Figure 23(b) shows that the implementation of the WA UDF in

ANSYS Fluent is not introducing any additional error for the first order discretization implementation.

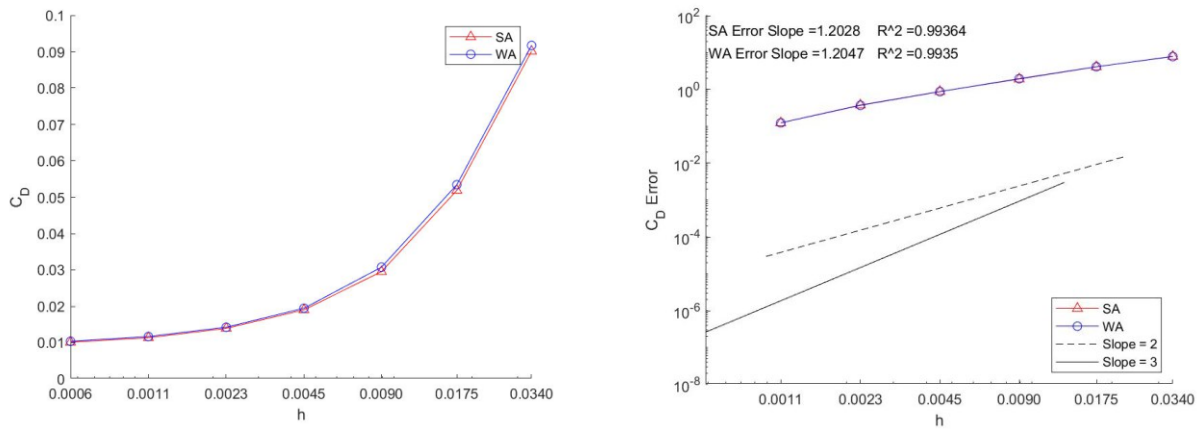

(a) Convergence of total drag coefficient

(b) Convergence of error in total drag coefficient

Figure 23: Grid and error ('w.r.t truth value') convergence study of the total drag coefficient, first-order solution.

Figure 24 shows the convergence of pressure and viscous drag coefficients. Both turbulence models over-predict and then converge to a value for the pressure drag. For the viscous drag prediction the WA model exhibits converge rate of 1.45, whereas the SA model exhibits convergence rate of approximately 1.1. The pressure drag coefficient follows the trend exhibited by the total drag coefficient shown in Fig. 24(c). Both the SA and WA model show convergence rate of 1.2 for the pressure drag prediction. Figure 24(d) shows that both the SA and WA model exhibit an approximately first order convergence rate.

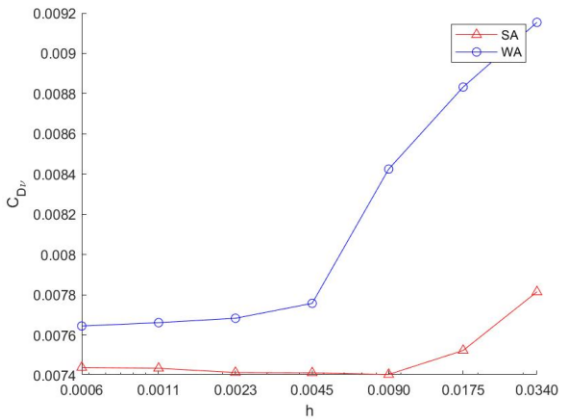

(a) Convergence of viscous drag coefficient

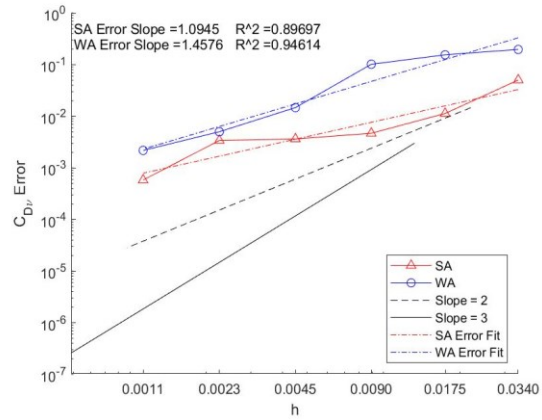

(b) Convergence of error in viscous drag coefficient

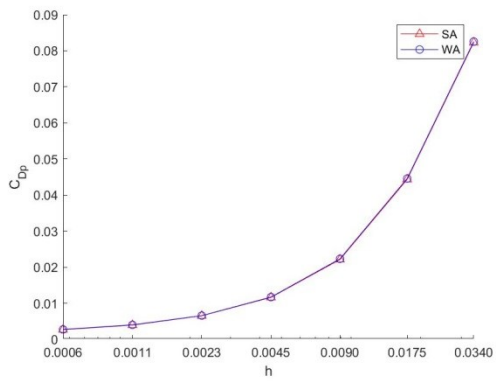

(c) Convergence of pressure drag coefficient

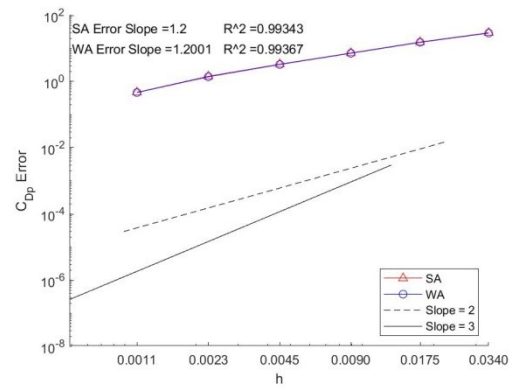

(d) Convergence of error in pressure drag coefficient

Figure 24: Convergence study of pressure and viscous drag coefficients, first-order solution.

5.3.2 Second-Order Solution on Hexahedral Meshes

This solution utilizes the second order upwind discretization for convection terms in the momentum, energy, and turbulent viscosity equations and second-order central-differencing for diffusion terms in these equations. A linear scheme is used for pressure. Since all equations except pressure have second order discretization, this solution method is expected to show nearly second order convergence.

Table 13 shows the second-order convergence results for the drag coefficient on the hexahedral mesh. N is defined as the number of 2D nodal points and h describes the nominal mesh spacing. Both turbulence models over- predict the drag coefficient and computations

converge to the "truth" value of drag coefficient on the finest mesh. The viscous drag coefficient does not change significantly using either model on different meshes. The pressure drag coefficient shows a similar trend in convergence toward the "truth" value as the total drag coefficient. Total drag coefficient is the sum of the viscous drag and the pressure drag. The "truth" value of drag coefficient is the value predicted using the finest mesh, grid #6 in Table 13.

Table 13: Convergence of total, pressure and viscous drag coefficients for second-order solution on grid #0 to grid #6.

Model	Grid	N	$h = N^{-1/2}$	C_D	C_{Dp}	C_{Dv}
	0	864	0.034021	0.042845959	0.035975769	0.006870191
	1	3264	0.017504	0.016247765	0.009151396	0.007096369
	2	12480	0.008951	0.009842096	0.002516838	0.007325257
SA	3	49536	0.004493	0.008964504	0.001550166	0.007414339
	4	197376	0.002251	0.00888675	0.001469663	0.007417087
	5	787968	0.001127	0.008883664	0.001438478	0.007445186
	6	3148800	0.000564	0.008913212	0.001464407	0.007448805
	0	864	0.034021	0.044522145	0.036391563	0.008130582
	1	3264	0.017504	0.017764333	0.009488515	0.008275818
	2	12480	0.008951	0.010546086	0.002670902	0.007875184
WA	3	49536	0.004493	0.009438456	0.001661064	0.007777392
	4	197376	0.002251	0.009217594	0.001508923	0.007708671
	5	787968	0.001127	0.009137206	0.001477033	0.007660173
	6	3148800	0.000564	0.009119596	0.00147151	0.007648086

As shown in Table 13, the total drag coefficient approaches the "truth" value of the drag coefficient as the mesh becomes finer. The "truth" value of the drag coefficient is the value predicted on the finest mesh (grid # 6). Figure 25 shows the total drag coefficient convergence curves for WA and SA model as the mesh becomes finer. Both models exhibit the same convergence trends for the drag coefficient. The error in solution on different meshes was calculated with respect to the "truth" value. Figure 25(a) shows the convergence behavior for the total drag prediction for the two models to be nearly identical. Again, the only difference in the total drag convergence curves is in the magnitude of the result, the total drag prediction from WA model is slightly higher than that predicted by the SA model. Figure 25(b) shows the WA and SA model exhibiting the similar second-order convergence trends in the error. Figure 25(b)

also indicates that the implementation of the UDF in ANSYS Fluent of WA model is not introducing any additional error.

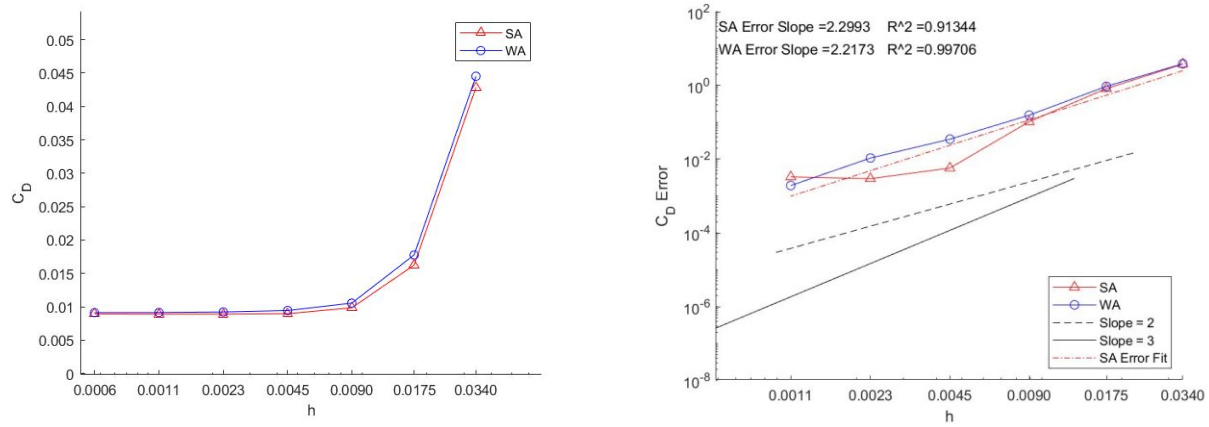

(a) Convergence of total drag coefficient

(b) Convergence of error in total drag coefficient

Figure 25: Grid convergence study of the total drag coefficient, second-order solution.

Figure 26 (a) and (c) show the convergence trends of viscous and pressure and drag coefficients respectively using the two turbulence models. The WA model over-predicts the viscous drag coefficient on coarser grids and then converges to a converged solution on grid #6, whereas the SA model under-predicts the viscous drag coefficient on coarser grids and then converges to a solution on grid #6. Figure 26 (b) shows that both models exhibit similar error convergence behavior for viscous drag coefficient. However, the error convergence curve for viscous drag shown in Fig. 26 (b) is more sporadic and exhibits a convergence trend less than second order. For pressure drag coefficient, both the models show almost identical convergence curves in Fig. 26 (c). Figure 26 (d) shows that both the SA and WA model exhibit similar error convergence curves for pressure drag. Overall, the pressure drag convergence trends are very similar to the total drag convergence trends.

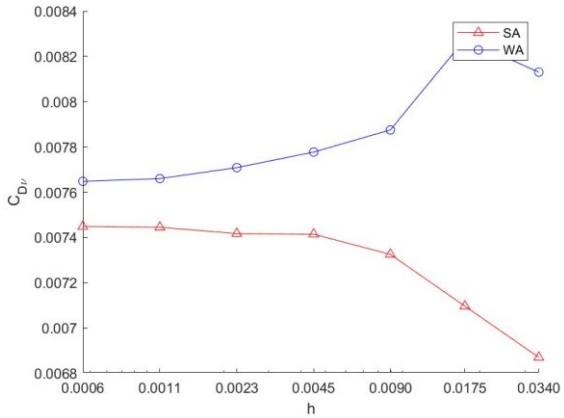

(a) Convergence of viscous drag coefficient

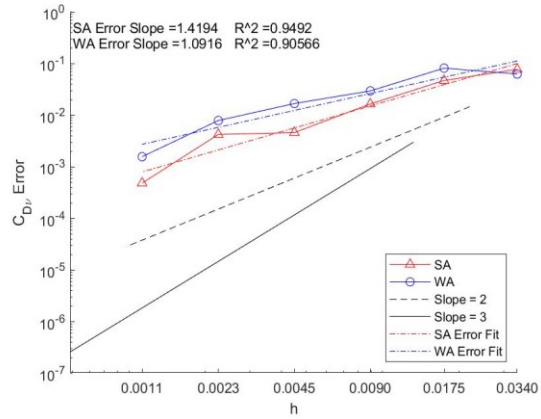

(b) Convergence of error in viscous drag coefficient

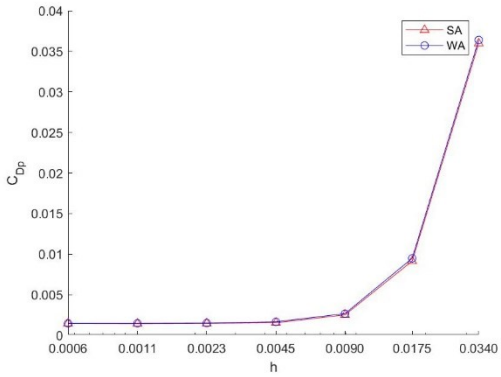

(c) Convergence of pressure drag coefficient

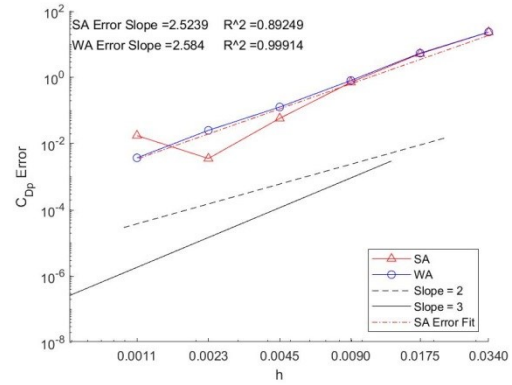

(d) Convergence of error in pressure drag coefficient

Figure 26: Convergence study of pressure and viscous drag coefficients, second-order solution.

5.4 Conclusions

This paper presents a convergence history of first-order and second-order accurate solutions of the Reynolds-Averaged Navier-Stokes (RANS) equations in conjunction with one equation standard Spalart-Allmaras (SA) and Wray-Agarwal (WA) turbulence models for computation of turbulent flow over Joukowski airfoil at Mach number = 0.15, Reynolds number Re = $3*10^6$ and angle of attack $\alpha = 0^o$. The results are presented for a family of seven meshes from coarse (grid #0) to fine (grid # 6) provided by the 2022 Joukowski airfoil High Fidelity CFD Workshop to the participants [1]. The Joukowski airfoil benchmark case was designed to evaluate the convergence properties of second- and higher-order accurate CFD solvers using the SA-[neg]

QCR 2000 turbulence model. In this paper, the solutions are obtained using the same solver – ANSYS Fluent with two different turbulence models, namely the standard SA model and WA 2017 model. The WA model exhibited nearly the same convergence rates as the SA model for both the first-order accurate and second order accurate solutions. The most notable differences in the predictions were found in the convergence of viscous drag coefficient using the two turbulence models. The WA model's convergence rates replicating the convergence rates of the SA model suggest that the UDF implementation of WA model in ANSYS Fluent does not introduce any additional numerical error.

5.5 References

[1] Galbraith, M., "High-fidelity CFD Workshop 2022: RANS SA-[neg]-QCR2000 Joukowski Airfoil Case,"AIAA 2022 SciTech Forum, https://turbmodels.larc.nasa.gov/Highfidelitycfd2021/Joukowski_HFW.pdf., 8-9 January 22.

[2] "The Wray-Agarwal Turbulence Model," NASA Langley Research Center Turbulence Model Resource Website URL: https://turbmodels.larc.nasa.gov/wray_agarwal.html.

[3] Spalart, P. and Allmaras. S., "A One-Equation Turbulence Model for Aerodynamic Flows," AIAA Paper 1992-439, 30th Aerospace Sciences Meeting and Exhibit, Reno, NV, 1992, URL: https://doi.org/10.2514/6.1992-439.

[4] Diskin, B., Ahmad, N., Anderson, W. K., Derlaga, J. M., Pandya, M. J., Rumsey, C. L., Wang L., Wood, S. L., Liu Y., Nishikawa, H. and Galbraith, M. C., "Verification Test Suite for the Spalart-Allmaras QCR2000 Turbulence Model," AIAA Paper 2021-1552, AIAA SciTech Forum, 2021, doi 10.2541/6.2021-1552.

[5] https://turbmodels.larc.nasa.gov/highfidelitycfd_workshop2022.html

Chapter 6: Summary

This thesis describes the turbulent and transitional flow solutions obtained for flow past NACA 0012, 0015 and 0018 airfoils using the Wray-Agarwal (WA) turbulence model and the Wray-Agarwal Algebraic Transition (WA-AT) model. In addition, it considers the CFD verification case proposed in the NASA/AIAA 2022 High Fidelity CFD Workshop – the flow past Joukowski airfoil using the WA model.

The computed results for turbulent flow past the symmetric NACA airfoils show the WA 2017 model predicts results for lift coefficient in good agreement with the results predicted by the Spalart-Allmaras model. The results also showed good agreement between the models' predictions and the experimental lift coefficient measurements. Investigations for airfoil flows at very high angles of attack in the stall regime and flow over airfoils with large camber should be conducted to further determine the capability of the WA 2017 model.

The Wray-Agarwal Algebraic Transition (WA-AT) model has shown competitive or better accuracy in prediction of flow past NACA 0012, 0015 and 0018 airfoils compared to the four equation transition SST (TSST) model when compared to experimental data. In some cases, for example for flow past NACA 0018 airfoil, the presence of laminar separation bubbles on the airfoils increases the difficultly in computing and verifying the computations for transitional flows. Based on the results overall, the WA-AT model has shown the potential to be a very promising single transport equation transition model. Being a one-equation model, it is computationally very efficient compared to three- and four equation SST transition models.

For the Joukowski airfoil CFD verification case in NASA/AIAA 2022 High Fidelity CFD workshop, the computed results using the Wray-Agarwal 2017 turbulence model show similar

convergence behavior for the total drag, pressure drag, viscous drag and error in total drag as the SA model on workshop specified seven grids from coarse to fine using both the first-order and second-order numerical algorithms.

It should be noted that WA 2017 model and WA-AT model are implemented in Fluent using a User Defined Function (UDF) while the SA modal and transition SST (TSST) model are a part of the FLUENT software. The results suggest that UDFs are not introducing additional error and have been implemented correctly.

Appendix A

The following tables present the tabulated results for the NACA 0012, 0015, and 0018 airfoils for the transitional flow cases.

Table A1 NACA 0012 transition flow tabulated results, Re 3*10^6, μ_t/μ = 100, Tu = 0.3%.

Turbulence Model	AOA	C_L	C_D	Transition location (x/c)
TSST	0	-9.01E-07	0.00471963	0.6
	2	0.2198296	0.00572672	0.36
	3	0.32661941	0.00533548	0.32
	4	0.43465237	0.00578723	0.26
	5	0.54146999	0.00648139	0.165
	6	0.64515246	0.00761828	0.05
	8	0.8533137	0.00964355	0.015
	10	1.0588852	0.01210445	0.011
WA-AT	0	3.14E-06	0.00578034	0.47
	2	0.22204394	0.00598664	0.34
	3	0.32984218	0.00654529	0.217
	4	0.44200716	0.0068122	0.206
	5	0.54843356	0.0073955	0.137
	6	0.65519902	0.00847379	0.072
	8	0.86248635	0.01020118	0.014
	10	1.0635072	0.01247696	0.008

Table A2 NACA 0015 transitional flow tabulated results, Re = 6*10^6 Case, Tu = 0.108%, μ_t/μ = 10.

Turbulence Model	AOA	C_L	C_D	Transition Location (x/c)
TSST	0	7.37E-07	0.005394	0.425
	2	0.215956	0.006198	0.22
	4	0.434696	0.006747	0.13
	6	0.651437	0.007615	0.091
	8	0.870053	0.009341	0.05
	10	1.06777	0.010325	0.03
WA-AT	0	-1.36E-07	0.006072	0.35
	2	0.226594	0.006468	0.26
	4	0.447136	0.007001	0.17
	6	0.667095	0.00803	0.1
	8	0.873294	0.010122	0.04
	10	1.084401	0.011431	0.03

Table A3 NACA 0015 transitional flow tabulated results, Re = 3*10^6 , Tu = 0.098%, μ_t/μ = 10.

Turbulence Model	AOA	C_L	C_D	Transition Location (x/c)
TSST	0	5.6651521e-08	0.0051741066	0.5500
	2	0.21998652	0.0059793972	0.3700
	4	0.43817841	0.0064865993	0.2800
	6	0.65133202	0.007707881	0.1500
	8	0.85256857	0.0091668691	0.0500
	10	1.0510434	0.011239622	0.0350
WA-AT	0	-1.468767e-06	0.0055358007	0.5200
	2	0.21509448	0.0062635283	0.2800
	4	0.43809594	0.0065048828	0.2400
	6	0.64811037	0.0080041094	0.1200
	8	0.86221678	0.0092399765	0.0600
	10	1.0924025	0.012164427	0.0330

Table A4 NACA 0018 transitional flow tabulated results, Re 1*10^6, Tu = 0.07%, μ_t/μ = 10.

Turbulence Model	AOA	C_L	C_D	Separation Location (x/c)	Reattachment/ Transition Location (x/c)
TSST	0	-1.30E-06	0.006890073	0.5	0.65
	2	0.20889811	0.007121987	0.38	0.52
	4	0.41538515	0.007877327	0.285	0.4
	6	0.61411279	0.009285973	0.19	0.24
	8	0.81379682	0.011594426	0.11	0.15
	10	1.0234935	0.014614489	0.06	0.1
WA-AT	0	-3.35E-07	0.006805305	0.475	0.61
	2	0.21173741	0.007060751	0.36	0.5
	4	0.42610663	0.008021787	0.28	0.38
	6	0.63982073	0.009464186	0.2	0.28
	8	0.86423874	0.011977665	0.12	0.18
	10	1.1287673	0.01520131	0.06	0.1